Skeletal stem cell isolation: A review on the state-of-the-art microfluidic label-free sorting techniques

Miguel Xavier, Richard O.C. Oreffo, Hywel Morgan

PII: S0734-9750(16)30065-9
DOI: doi: 10.1016/j.biotechadv.2016.05.008
Reference: JBA 7051

To appear in: *Biotechnology Advances*

Received date: 3 March 2016
Revised date: 13 May 2016
Accepted date: 22 May 2016

Please cite this article as: Xavier Miguel, Oreffo Richard O.C., Morgan Hywel, Skeletal stem cell isolation: A review on the state-of-the-art microfluidic label-free sorting techniques, *Biotechnology Advances* (2016), doi: 10.1016/j.biotechadv.2016.05.008

Skeletal Stem Cell Isolation: A Review on the State-of-the-Art Microfluidic Label-Free Sorting Techniques

Miguel Xavier[a,b], Richard OC Oreffo[b] and Hywel Morgan[a,*]

[a] Faculty of Physical Sciences and Engineering, Institute for Life Sciences, University of Southampton SO17 1BJ, United Kingdom.

[b] Centre for Human Development, Stem Cells and Regeneration, Institute of Developmental Sciences, Southampton General Hospital, Tremona Road SO16 6YD Southampton, United Kingdom.

[*] Corresponding author at: Office 2105, Building 85, Institute for Life Sciences, Highfield Road, University of Southampton SO17 1BJ, United Kingdom.

Author e-mails (by order of appearance): j.xavier@soton.ac.uk; roco@soton.ac.uk; hm@esc.soton.ac.uk

Abbreviations: SSC, skeletal stem cells; bone marrow, BM; mesenchymal stem cells, MSCs; bone marrow stromal cells, BMSCs; bone marrow aspirates, BMA; CFU-F, colony forming unit-fibroblastic; fluorescence/magnetic-activated cell sorting, FACS/MACS; circulating tumour cells, CTCs; deterministic lateral displacement, DLD; dielectrophoresis, DEP; geometrically-enhanced differential immunocapture, GEDI; white blood cells, WBC; red blood cells, RBC; quadrupole magnetic flow sorter, QMS; haematopoietic stem cells, HSC; peripheral blood progenitor cell, PBPC; field-flow fractionation, FFF; real-time deformability cytometry, RT-DC.

Abstract

Skeletal stem cells (SSC) are a sub-population of bone marrow stromal cells that reside in postnatal bone marrow with osteogenic, chondrogenic and adipogenic differentiation potential. SSCs reside only in the bone marrow and have organisational and regulatory functions in the bone marrow microenvironment and give rise to the haematopoiesis-supportive stroma. Their differentiation capacity is restricted to skeletal lineages and therefore the term SSC should be clearly distinguished from mesenchymal stem cells which are reported to exist in extra-skeletal tissues and, critically, do not contribute to skeletal development.

SSCs are responsible for the unique regeneration capacity of bone and offer unlimited potential for application in bone regenerative therapies. A current unmet challenge is the isolation of homogeneous populations of SSCs, *in vitro*, with homogeneous regeneration and differentiation capacities. Challenges that limit SSC isolation include a) the scarcity of SSCs in bone marrow aspirates, estimated at between 1 in 10-100,000 mononuclear cells; b) the absence of specific markers and thus the phenotypic ambiguity of the SSC and c) the complexity of bone marrow tissue.

Microfluidics provides innovative approaches for cell separation based on bio-physical features of single cells. Here we review the physical principles underlying label-free microfluidic sorting techniques and review their capacity for stem cell selection/sorting from complex (heterogeneous) samples.

Keywords: Skeletal stem cells; Microfluidics; Label-free; Cell sorting; Cell separation; Human bone marrow; Bone regeneration

1. Introduction

Current estimates indicate that in developed countries the majority of children born after the millennium will live to witness their 100th birthday (Christensen et al., 2009). While this heralds a significant achievement for global health and medical care, such advances in longevity are typically accompanied with exacerbated health problems and increased demands for personalised, directed and effective regenerative therapies (Christensen et al., 2009; Rachner et al., 2011). Within the musculoskeletal arena, increased bone trauma and bone disease are associated with advancing years and stem cell-based therapies have been suggested as a possible approach to address these issues (Bianco, 2015; Dawson et al., 2014; Rachner et al., 2011).

Bone has unique capacity for regeneration, indicating the potential of a multipotent stem cell resident in the bone with the capacity to support bone tissue engineering, skeletal stem cell transplantation or pharmacological studies targeting bone disease (Bianco, 2015). Indeed, almost half a century ago, Friedenstein and colleagues, first documented the occurrence of osteogenesis in heterotopic transplants of bone marrow (BM) stromal cells *in vivo*, providing evidence of a stem cell with the capacity to generate bone (Friedenstein et al., 1968, 1966). BM stroma-derived cell populations with replicative and differentiation capabilities are typically referred to as mesenchymal stem cells (MSCs). However, this term has proved itself to represent a highly heterogeneous cell population when these cells are grown *in vitro*, comprising often several progenitor cells for different terminal cell lineages. The heterogeneous population of cultured plastic adherent cells isolated from the bone marrow, widely used in the community to study bone reparation, will be referred to as bone marrow stromal cells (BMSCs). The term skeletal stem cell (SSC), proposed by Friedenstein and Owen, is used in this review to refer specifically to the self-renewing stem cell of the bone marrow stroma responsible for the regenerative capacity inherent to bone. The SSC displays osteogenic, chondrogenic and adipogenic differentiation potential *in vivo* and the capacity to form a functional BM-haematopoietic microenvironment (Bianco, 2015; Bianco and Robey, 2015; Friedenstein et al., 1968, 1966; Friedenstein and Owen, 1988; Gothard et al., 2011).

Current SSC isolation and purification techniques usually rely on density centrifugation of BM aspirates (BMA) followed by culture adherence to tissue culture polystyrene. At clonal seeding densities, the formation of distinct colonies, named colony forming units-fibroblastic (CFU-F) can be observed, a fraction of which (approximately 15%), contains the SSC sub-population. The skeletal stem cell population is thought to be of pericyte origin and to reside *in vivo* over the BM sinusoids (Bianco, 2015; Gothard et al., 2011; Janeczek et al., 2015a). In theory, one single stem cell is sufficient for application in stem cell regenerative therapies due to their accepted replicative capacity. However, a key challenge hampering clinical translation is the necessity to enrich/obtain, *in vitro*, a sufficient population of cells with a homogeneous regeneration and differentiation capacity (Gothard et al., 2011; Poon et al., 2014). Critically, expansion *ex vivo* can contribute to an increase in cell heterogeneity linked to a loss of proliferative and differentiation capacity (Gothard et al., 2011). To date, researchers have struggled to develop isolation techniques that will provide SSC populations of sufficient high purity and cell yield without compromising cell viability.

Although a specific marker for the SSC remains elusive, positive-selection based on the application of one or more SSC-surface markers using fluorescence- or magnetic-activated cell sorting (FACS and MACS), is widely used. One commonly used approach is density centrifugation followed by MACS separation using positive-selection of Stro-1^{+} (a putative SSC marker with some 10-15% reactivity of BMSCs) cells and plastic adherence to enrich for SSCs (Gothard et al., 2014, 2013).

Limitations in SSC isolation techniques are related to a) the scarcity of SSCs in BMA (1 in 10-100,000 mononuclear cells) (Jones and McGonagle, 2008), b) the absence of specific markers and thus the phenotypic ambiguity of the SSCs (Bianco et al., 2013; Gothard et al., 2014, 2011; Tare et al., 2008) and, c) the complexity of bone marrow tissue with cell types displaying overlapping features to the SSCs (Fawcett and Bloom, 1994; Junqueira and Carneiro, 2005). To address some of these issues, microfluidic technologies offer new routes for single cell analysis and high throughput cell sorting that do not rely on cell-surface markers but rather on distinct cell phenotypic features. This review summarises recent advances in microfluidic sorting techniques and their potential applicability to the isolation of pure and homogeneous SSC populations for academic and clinical applications.

2. State-of-the-art cell isolation techniques and their caveats for skeletal stem cell sorting

The main approaches employed in SSC sorting are fluorescence and magnetic cell sorting combined with plastic culture adherence (Tare et al., 2008). Herzenberg and his colleagues first described fluorescent activated cell sorting (FACS) in 1972 (Bonner et al., 1972), whilst Miltenyi Biotec developed magnetic sorting and registered the trademark MACS (Miltenyi et al., 1990). Both depend on the use of antibodies to specific antigens that are either present on the cell membrane, or in the cell cytoplasm or even nucleus. Cell sorting is performed using either positive or negative selection depending on whether the cells targeted by the antibodies are those of interest or the contaminants. The principle of separation differs depending on the method employed. In FACS, cells are suspended in droplets and sorted depending on the presence or absence of a fluorescent tag. MACS uses magnetic beads attached to a primary antibody allowing tagged cells to be retained within a flow-through device by a strong magnetic field (Plouffe et al., 2015).

FACS can process thousands of cells per second in a serial manner, and provides the possibility of selection based on targeting intracellular components, multiple antigens, or antigen density. MACS is a bulk cell sorting technology and is fluorescence-independent. In theory, both FACS and MACS should be able to isolate 100% pure cell populations if appropriate cell specific selection markers are available. However, cost (reagents, antibodies, flow cytometer), time (typically 7-8 hours protocols with possible loss of cell viability as a consequence) and the need for trained personnel are considerable limitations for both techniques (Karabacak et al., 2014; Plouffe et al., 2015). Nevertheless, the major hurdle in the application of FACS or MACS for SSC sorting is the lack of a specific cell marker for the SSC. For example, the widely used antibody Stro-1 reacts with approximately 10-15% of BMSCs and provides only enrichment rather than selection of SSCs.

Stro-1 was first identified by Simmons and Torok-Storb in 1991 and is a relatively widely used marker for SSC sorting and analysis, and for selection of high growth-potential CFU-Fs (Kolf et al., 2007; Lin et al., 2011; Simmons and Torok-Storb, 1991; Tare et al., 2008). In 2003, Gronthos *et al.* obtained a 950-fold enrichment of CFU-Fs by MACS separation of Stro-1^{bright} human bone marrow stromal cells (Gronthos et al., 2003). Combining MACS with subsequent separation of $CD146^{+}$ cells by FACS, improved this to 2,000-fold (Shi and Gronthos, 2003). SSCs are described as being positive for the Stro-1 antigen as well as CD146, CD271, CD49a, CD63, CD71, CD73, CD90, CD105, CD106, CD166 or ICAM-1, while lacking the expression of haematopoietic markers such as CD45, CD34, CD11, CD14, and CD235a (Fig. 1)(Dawson et al., 2014; Tare et al., 2008; Zannettino et al., 2007).

(Please insert Figure 1 after this paragraph)

Finding a unique cell surface marker for SSC through peptide phage display or DNA libraries could provide the key for the isolation of homogeneous SSC populations using such conventional sorting techniques (Gothard et al., 2011). However, while this search continues, solutions may also lie in approaches which do not rely on antibody selection, but rather on other physical properties such as size, deformability, membrane roughness or cell acoustic and dielectric properties. Label-free strategies are also attractive as they deliver cells in an unaltered and unperturbed state for further analysis or application (Lara et al., 2004).

Microfluidics is an ideal platform for single cell analysis and has been used for sorting rare cell populations such as circulating tumour cells (CTCs) with high throughput, purity and recovery rates (Beech et al., 2012; Gascoyne and Shim, 2014; Gossett et al., 2010; Karabacak et al., 2014; Ozkumur et al., 2013). Microfluidic approaches for cell separation include techniques such as inertial focusing, deterministic lateral displacement (DLD), dielectrophoresis (DEP), acoustophoresis or magnetophoresis. In this paper, each of these techniques is briefly reviewed emphasising their potential application to stem cell sorting. Tables 2 and 3 summarise examples of each technique for sorting stem or progenitor cells and CTCs, respectively.

3. Microfluidic techniques for cell sorting applications

3.1. Affinity-based

Microfluidics has led to the development of high efficiency affinity-based sorting of cells from heterogeneous samples. One of the first and most significant publications that used microfluidics and immunocapture was the CTC-chip (Nagrath et al., 2007). It consisted of 78,000 epithelial cell adhesion molecule (EpCAM) antibody-functionalised cylindrical microposts that increased the surface area of the device approximately 3-fold and promoted cell-antibody interactions. The posts (100 µm wide and 100 µm high) were arranged in an equilateral triangular array, which was shown by simulation to be the most hydrodynamically efficient geometric arrangement and also to create non-linear streamlines promoting cell contact with the antibody. Every 3 rows the posts were shifted vertically to ensure that cells following streamlines between the microposts (as predicted by simulation, Fig. 2a) were forced to collide with posts located downstream. The device was operated at a flow rate of 1-2 mL/h to ensure maximum cell-antibody interaction whilst limiting shear forces to maximise the probability of attachment. Under these conditions, more than 60% of all CTCs spiked in whole blood could be recovered, demonstrating detection of CTCs in 115 out of 116 cancer patients from disparate cancer backgrounds: lung, prostate, pancreatic, breast and colon cancer (Maheswaran et al., 2008; Nagrath et al., 2007; Stott et al., 2010b). Applying a different principle, the same group later developed the herringbone-chip, which increases the probability of cell-antibody interaction through passive mixing of blood cells caused by the generation of micro-vortices from the chevrons on the device surface (Fig. 2b) (Stott et al., 2010a). The device was able to recover more than 90% of the CTCs spiked in whole blood and could detect CTCs from 93% of cancer patient samples. More recent implementations of this device using different antibody cocktails allowed capture of breast, prostate and pancreatic CTCs. These cells were processed on-chip to conduct phenotypic and even molecular (*e.g.* through single-molecule RNA sequencing analysis) characterisation studies answering important questions on the mechanisms and therapy of cancer metastasis (Miyamoto et al., 2012; Yu et al., 2013, 2012).

(Please insert Figure 2 after this paragraph)

Kirby's group developed devices that improved the efficiency of antibody cell capture by maximising the frequency of interaction of larger target cells, using antibody-functionalised silicon micro-structures that induce size-dependent collisions (Gleghorn et al., 2010). These devices, termed geometrically-enhanced differential immunocapture (GEDI), are designed to distort streamlines so that the cell displacement caused by impact with obstacles increases the probability of future impacts for larger cells, such as CTCs, more than for smaller cells, such as white blood cells (WBCs) (Fig. 2c). The obstacle shape and array geometries can be tuned to address specific cell size thresholds depending on the application (Fig. 2d). GEDI devices were able to recover over 85% of prostate CTCs spiked into whole blood and detected CTCs from the peripheral blood of 18 out of 20 patients, at a processing rate of over ten million cells per minute (Gleghorn et al., 2010). GEDI devices have also been shown to isolate breast and gastric cancer cells (Galletti et al., 2013), and enable on-chip functional characterisation of CTCs (Kirby et al., 2012; Thege et al., 2014). The GEDI principle has also been coupled with DEP to further increase the probability of antibody interaction (Huang et al., 2013; Smith et al., 2015).

Finally, as an example of an affinity-based approach applied to progenitor cells, one study has reported encapsulation of cells retrieved from digested human periosteal tissue into microscale water in oil droplets, generated using a T-junction microfluidic flow. The encapsulated cells were analysed on the same device using a micro-FACS system that incorporates two aligned laser beam sources (488nm and 635 nm) focused through a 60x water-immersion objective, identifying Stro-1^{+}-labelled progenitor cells

(Srisa-Art et al., 2009). Although this was not a sorting device, it shows the potential for developing a novel cell sorting technology for rare stem cells.

The examples of affinity-based microfluidic sorting techniques shown above demonstrate encouraging performances in terms of efficiency and throughput, applicable for SSC sorting. However, some limitations must be accounted for, as for example, when used to positively select cells, the rare cells need to be released after capture. This can be challenging and some of the commonly used approaches such as the use of shear stress or enzymatic release can harm viable cells (Chen et al., 2014). However, important advances have recently been made using e.g. thermo- and mechano-sensitive smart polymers to increase release efficiency and cell viability (Reátegui et al., 2015; Yoon et al., 2016). In terms of applications to SSC isolation, positive selection will lead to impure populations owing to the absence of selective antibodies. Negative selection using affinity–based microfluidic techniques that capture contaminant cells on chip is generally inefficient for sorting rare cells as the devices can become clogged by the unwanted cells. Consequently, label-free microfluidic sorting techniques or methods offering continuous-flow negative selection for sorting SSCs, may well offer advantages over an immunocapture affinity-based approach.

3.2. Deterministic Lateral Displacement

Deterministic lateral displacement (DLD) was first described in 2004 (Huang et al., 2004). It has been developed as a tool for bioparticle sorting and is capable of high resolution fractionation, of the order of 2% in particle size, with the smallest particle size in the range of viruses (Huang et al., 2004; Morton et al., 2008) . DLD is a continuous flow sorting technique that separates cells based on size. A DLD device consists of consecutive rows of micrometre scale obstacles, commonly cylindrical in shape, and equally spaced (G), with each row shifted by a small distance horizontally (Δλ) with respect to the previous one as shown in Fig. 3. After N rows, two obstacles return to the exact same horizontal position and this defines the period of the array.

(Please insert Figure 3 after this paragraph)

The flow is laminar (Reynolds<1), so that viscous effects dominate over inertia. The main flow stream is split by the obstacle array into N parallel laminae with identical flow volumes. In Fig. 3 an example is given for a microarray with period N=3. When cells flowing in a streamline encounter an obstacle, they reach a critical decision point in which their behaviour is determined by the critical size of the microarray. This critical size (R_C) corresponds to the width of the streamline found closest to the obstacle, and for spherical particles (as most cells in suspension), this has been empirically determined as (Holm et al., 2011; Huang et al., 2004; McGrath et al., 2014; Morton et al., 2008):

$$R_C = 1.4G \times N^{-0.48} \quad (1)$$

At each decision point, if a cell's radius is smaller than the array critical size, the cell will be mostly affected by the first streamline and therefore remain unperturbed, zigzagging through the obstacle array. However, if a cell's radius is larger than the width of the first streamline, then more than half of the cell will be affected by the second streamline and the cell will be "bumped away" or, more correctly, laterally displaced. This phenomenon is repeated upon interaction with each post, so that cells with sizes larger than the critical size for separation will end up completely separated from the initial input flow (Holm et al., 2011; Huang et al., 2004; McGrath et al., 2014; Morton et al., 2008).

Several adaptations of the original DLD principle have been developed, sorting particles according to additional physical properties such as shape (Beech et al., 2012), deformability (Beech et al., 2012; Holmes et al., 2014), density (Holm et al., 2013), gravity (Devendra and Drazer, 2012), acoustic (Collins et al., 2014) and dielectric properties (Beech et al., 2009; Collins et al., 2014). The basic rationale is that an additional force changes the effective radius (and/or trajectory) of a particle. For instance, at high pressures, a more deformable particle is squeezed by the shear forces upon interacting with the posts making it appear smaller (Beech et al., 2012). Beech *et al*. explored these effects to show how different red blood cells (discocytes, stomatocytes and echinocytes), have different deformability profiles (Beech et al., 2012). More recently, the same principle was applied to sort T-lymphocytes from neutrophils according to differences in cell stiffness (Holmes et al., 2014).

To date, DLD has been used to sort many different particles, including beads, bacteria, parasites and WBCs, red blood cells (RBCs) and platelets from blood. See McGrath *et al.* for a review (McGrath et al., 2014). There are no examples of stem cell sorting by DLD. One application regarding tissue engineering purposes is the use of DLD to separate two immortalised cell lines, one fibroblastic and one epithelial, mixed in equal proportions to mimic cardiomyocytes and nonmyocytes from a cardiac tissue digest (Green et al., 2009). The same group also demonstrated isolation of cardiomyocytes from primary cardiac tissue digests with a purity of 91% (Zhang et al., 2012). However, the throughput was relatively low (~20,000 cells/min) and the recovery efficiency of cardiomyocytes in the positive fraction was only 30-35%. High throughput is clearly important for sorting rare cell populations such as SSCs from bone marrow, where large sample volumes and cell numbers must be analysed. Likewise, recovery efficiencies need to be maximised to avoid losing rare target cells.

Traditional DLD devices operate typically at flow rates of less than one to a few microliters per minute and require sheath flow which introduces significant dilution of the sample at the outlets (McGrath et al., 2014). To improve throughput, devices can be operated in parallel and/or without using sheath flow. Of relevance to sorting SSCs, Inglis *et al.* (Inglis et al., 2011) showed a 10-fold enrichment of leukocytes from whole blood, with 98% recovery efficiency. Blood samples were sorted undiluted, increasing volumetric throughput to 115 µL/min when using a device with 6 parallel DLD arrays.

Sheathless DLD devices have also been developed for sorting rare cells. In the examples below, two mirrored DLD arrays with triangular posts were used to displace the target cells and concentrate them in the centre of the device for collection. Breast and prostate cancer cell lines spiked (1:300) into (1:20) diluted blood were separated at flow rates of 10 mL/min (Loutherback et al.,

2012). A recovery efficiency of 86% was reported, but as many as 5 in every 100 cells in the input were cancer cells and the output was highly contaminated with blood cells (>80%) (Fig. 3b). Despite the high fluid velocities achieved (~1.5 m/s) the cells were shown to remain viable after separation. Liu *et al.* (Liu et al., 2013) sorted two breast cancer cell lines spiked at a ratio of 1:10,000 in 1:10 diluted blood. Isolation efficiencies of 99% and 80% were achieved at a flow rate of 2mL/min, giving a higher efficiency at similar throughput as the rare cells were significantly more diluted (Fig. 3c).

A high throughput DLD system used for de-bulking and pre-processing samples uses 24 parallel mirrored arrays (Fig. 3d). It can process blood to remove RBCs and platelets at flow rates of up to 8mL/h (Huang et al., 2008; Karabacak et al., 2014; Ozkumur et al., 2013). Combining DLD with subsequent magnetophoretic sorting based on the intrinsic magnetic susceptibility of the haemoglobin-positive progenitor nucleated RBCs found in the peripheral blood of pregnant women showed enrichment by over 1,000-fold (Huang et al., 2008). Recently, DLD has been combined with magnetic-bead based depletion of $CD45^+$ and $CD66b^+$ WBCs, for CTC isolation, achieving 97% recovery from patient samples, whilst removing all RBCs depleting the WBCs by a 3.8-log ratio (Karabacak et al., 2014).

While the volumetric and cell sorting throughputs reported above are adequate for sorting SSCs from human bone marrow, size differences on their own won't be sufficient to sort SSCs by DLD. Nevertheless, DLD may be used as a passive, efficient and relatively simple procedure to decomplex bone marrow samples prior to further selection by an additional sorting technique, as exemplified by the works shown above.

3.3. Magnetophoresis

Magnetophoresis is a sorting technique that uses a magnetic field to manipulate magnetic particles. For example, cells can be sorted according to their intrinsic magnetic susceptibility or based on superparamagnetic nanoparticles covalently bound to labelling antibodies – a method termed immunomagnetic sorting. This method is similar to MACS, is usually not label-free and, requires highly specific antibodies (Plouffe et al., 2015).

Nevertheless, this technique has been miniaturised into microfluidic devices bringing the advantage of scale. Specifically it is much easier to generate well defined, high magnetic field gradients on the micron-scale. Furthermore, when used for negative depletion of contaminant cells it does not depend on the specific expression of a certain antigen by the cells of interest, like Stro-1 or CD146 in SSCs. It has been used for improving the purity of a desired cell population in continuous-flow, in combination with DLD (Huang et al., 2008; Karabacak et al., 2014; Ozkumur et al., 2013). A similar approach could be applied as a sorting strategy for SSCs, where contaminating cells like monocytes, are often found in the final SSC cultures since they are mononuclear, and can adhere to tissue culture polystyrene. Monocyte depletion could be achieved by negative depletion with CD14 or CD45 antibodies since neither are expressed by SSCs.

In magnetophoresis, cell movement depends on the different forces acting on it, which in a continuous flow comprise magnetic, buoyancy, inertial and drag forces. The magnetic force will depend on the volume of the magnetic particle (V_p), the difference between the magnetic susceptibility of the particle and the suspending medium ($\Delta\chi$), and the square of the magnetic field gradient ($(\vec{B}.\nabla)\vec{B}$), with μ_0 being the permeability of free space: (Plouffe et al., 2015)

$$\vec{F}_m = \frac{V_p \nabla \chi}{\mu_0}\left(\vec{B}\cdot\nabla\right)\vec{B} \quad (2)$$

As the magnetic susceptibility of the suspending medium is usually several orders of magnitude lower than the magnetic particles used for sorting, the magnetic susceptibility is often determined by that of the particles alone (Plouffe et al., 2015). When labelling cells with antibody-coated magnetic beads, the equation can be modified to accommodate the number of magnetic beads on the cell surface that are conjugated to the desired antibody (β), the number of cell-surface markers targeted (n), the fraction of these which was bound by the antibody (θ) and the number of antibodies which can bind to a single marker (λ) as follows (Plouffe et al., 2015):

$$\vec{F}_m = \frac{V_p \nabla \chi \beta n \theta \lambda}{\mu_0}\left(\vec{B}\cdot\nabla\right)\vec{B} \quad (3)$$

Applications of magnetophoresis can be grouped into three categories: conventional MACS systems (Fig. 4a), still the gold standard in magnetic separation, the quadrupole magnetic flow sorter (QMS) (Fig. 4b) and microfluidic-magnetophoretic applications. The concept of QMS was introduced by Zborowski *et al.* in 1999 (Zborowski et al., 1999). It uses four permanent magnets to create a quadrupole magnetic field with a centrifugal character deviating magnetic-labelled cells from a central stream into the channel periphery, later separated by a flow splitter (Fig. 4b) (Zborowski et al., 1999). Advantages of the QMS are its high throughput and recovery efficiencies, sorting over 10^6 cells per second while retaining 95% of the target cells (Plouffe et al., 2015).

(Please insert Figure 4 after this paragraph)

Significant applications of the QMS include those from Chalmers and Zborowski's group in which human $CD34^+$ progenitor cells were sorted from peripheral blood samples by negative selection of leukocytes labelled with a tetrameric antibody cocktail (Jing et al., 2007) or an anti-CD3 antibody (Tong et al., 2007), achieving up to 4-log depletion of leukocytes without the need for labelling the progenitor cells. Sorting CTCs by negative depletion of $CD\text{-}45^+$ cells after RBC-lysis, Yang *et al.* reported a 2.9 log-depletion of leukocytes and a 5.7 log-depletion of total blood cells from peripheral blood samples of cancer patients while recovering an average of 22 CTCs per millilitre of blood (Yang et al., 2009). Another interesting application by the same group

concerns debulking of blood by depletion of RBCs down to 5% of their initial value simply relying on their intrinsic magnetic susceptibility (Moore et al., 2013).

Microfluidic magnetophoretic systems have been used for positive selection of labelled-cells for many years, and these devices are commonly referred to as micro-MACS (μMACS). When an antibody with high specificity is used, high recovery efficiencies are possible with excellent depletion of contaminating cells at high throughput. The work of Plouffe *et al.* (Plouffe et al., 2012) and Huang *et al.* (Huang et al., 2012) are two good examples in which the throughput was of the order of hundreds of millions to a billion cells per minute. Plouffe *et al.* (Plouffe et al., 2012) reported recovery of spiked CTCs or primary haematopoietic stem cells (HSCs) from whole blood with efficiencies of 88% and 97%, whilst Huang *et al.* (Huang et al., 2012) successfully detected CTCs from cancer patients with recovery efficiencies rounding 60% to 70%.

Given the lack of a specific marker for SSC, the negative selection magnetophoresis approach is of interest. The work from Toner's lab is notable for achieving a 3.8 log-depletion of WBCs and CTC recovery efficiencies rounding 97% from undiluted whole blood (Karabacak et al., 2014; Ozkumur et al., 2013). The magnetophoretic stage of the system is able to continuously sort over $5x10^5$ cells/min. To maximise efficiency, both labelled and unlabelled cells are aligned in the magnetic field by inertial focusing after the DLD debulking step (Fig. 4c). The magnetically-labelled WBCs are deflected from the focused streams in two serial stages. In the first stage, the cells travel faster and are subjected to a low magnetic field gradient which typically deflects 99.9% of all WBCs. The WBCs are deflected to the centre of the channel rather than onto the channel walls in order to minimise the formation of cell aggregates. At the second stage, the cell speed is slower, increasing residence time, and the magnetic field gradient is increased. This provides a higher force, deflecting WBCs labelled with fewer than 7 magnetic beads per cell, *ergo* increasing purity.

Two publications describe devices that are completely label-free. Taking advantage of the paramagnetic nature of deoxyhaemoglobin RBCs, over 93% were removed from diluted whole blood whilst retaining 97.4% of WBCs, resulting in a 15-fold enrichment (Han and Frazier, 2006). Huang *et al.* (Huang et al., 2008) applies the same principle to sort nucleated RBCs (nRBCs) from the peripheral blood of pregnant women for diagnosis of maternal and foetal health. DLD was used in a first stage to remove RBCs and platelets from diluted blood at $6x10^8$ cells/min. The sample, now deprived of 99.99% of the RBCs, flows through a magnetic column which removes 99.9% of all haemoglobin-negative cells, resulting in a total enrichment over 10^3-fold. Using this system, nRBCs were sorted in 58 out of 58 patients. Note that the nucleated erythroid cells represent 95% of the Stro-1 expressing cells in the bone marrow (Simmons and Torok-Storb, 1991), representing the biggest contaminant population when isolating Stro-1^+ SSC by MACS. As the erythroid cells are non-adherent, they can be easily removed after adhesion of the SSCs to culture flasks. However, this may be an issue in cases where SSCs are needed immediately.

3.4. Inertial Microfluidics

For Reynolds numbers in the range of 1 to 100 flow remains laminar but inertial forces begin to play an increasingly important role in determining the behaviour of both flowing cells and their suspending medium (Amini et al., 2014). The use of inertial effects to manipulate cells has resulted in several applications for cell focusing and sorting, as well as sample decomplexing, which have been reviewed by others (Amini et al., 2014; Carlo, 2009; Geislinger and Franke, 2014).

Inertial microfluidics generates forces acting on particles perpendicular to the main direction of flow. In general two counteracting forces are responsible for the inertial forces. The first is exerted by the presence of a boundary, usually the channel wall. The disturbance of the flow field by the cell and the reflection of this disturbance at the closest wall will direct the cell away from it. In addition, a velocity gradient in the parabolic profile of Poiseuille flow induces a shear gradient lift force, which draws the particle away from the centre of the channel. For a cell of radius (r_c) flowing in a channel with hydraulic diameter (D_h), and when the ratio of (r_c/D_h) is in the range 0.05 and 0.2, the wall and shear gradient lift forces are proportional to equations 4 and 5 (Amini et al., 2014; Di Carlo et al., 2009; Geislinger and Franke, 2014).

$$F_{L_W} \propto \frac{\rho U^2 r_c^6}{{D_h}^4} \quad (4) \qquad F_{L_{S-G}} \propto \frac{\rho U^2 r_c^3}{D_h} \quad (5)$$

Here *U* and ρ are the average flow velocity and the suspending medium mass density, respectively. When these two forces match, the particle is focused to an equilibrium position as shown schematically in Fig. 5a. Neutrally buoyant spherical particles flowing in a cylindrical channel spontaneously focus at an annulus with a radius of 0.6 times that of the channel (Fig. 5b) (Segré and Silberberg, 1961). For square or rectangular channels, particles focus into 4 or 2 symmetric equilibrium positions, respectively (Fig. 5b) (Amini et al., 2014). Note that inertial focusing is a strong function of particle to channel size ratio and also particle concentration due to particle-particle hydrodynamic interactions (Amini et al., 2014; Di Carlo et al., 2009). The rheological properties of the fluid, the particle shape and also deformability can affect the lift force thereby causing particles to focus at different positions. For example, discoid deformable particles, such as RBCs in whole blood, experience a net lift force towards the centre of the channel, as described by the Fårhaeus-Lindqvist effect (Fig. 5c) (Amini et al., 2014; Fåhræus and Lindqvist, 1931; Geislinger and Franke, 2014).

(Please insert Figure 5 after this paragraph)

Particle manipulation by inertial microfluidics can be further modified by the introduction of different structures into the micro-channels, such as curves, grooves, pillars, herringbones or different cross-sections (Amini et al., 2014; Carlo, 2009; Carlo et al., 2007; Martel and Toner, 2013; Stroock et al., 2002). Curved channels for instance, introduce additional effects into the system

due to the formation of a secondary flow, known as Dean Flow, which arises from the fact that the fluid has to travel different distances along the inner and outer sides of a curved channel resulting in different velocity profiles at different radial positions. A set of secondary flows named Dean vortices are formed, with fluid near the centre of the channel travelling outwards while fluid near the top and bottom walls travels inwards to compensate and conserve mass (Fig. 5d) (Amini et al., 2014; Carlo, 2009; Kuntaegowdanahalli et al., 2009; Martel and Toner, 2013). This leads to lateral migration of cells by the introduction of a Dean drag resulting in the alteration of the initial inertial equilibrium focusing positions. The magnitude of these forces is estimated through a dimensionless number, the Dean number (De, equation 6) (Geislinger and Franke, 2014), and the force experienced by a cell is approximated by the expression in equation 7: (Geislinger and Franke, 2014)

$$De = Re\sqrt{\frac{D_h}{2R_{curve}}} \quad (6) \qquad F_D = 5.4 \times 10^{-4}\pi\mu De^{1.63} r_c \quad (7)$$

Here R_{curve} is the radius of the channel's curvature and μ the suspending medium viscosity. Particles with different sizes will therefore focus to unique equilibrium positions depending on the ratio of lift and drag forces (Fig. 5d). The Dean force should not be confused with centrifugal forces, which arise from a density mismatch between particle and fluid, and are often negligible in microfluidics (Amini et al., 2014; Carlo, 2009; Carlo et al., 2007; Kuntaegowdanahalli et al., 2009; Martel and Toner, 2013).

Inertial microfluidics has been successfully used for sorting progenitor cell populations. Recently, Poon *et al.* designed a microfluidic spiral channel with a trapezoidal cross-section to perform binary fractionation of human BMSCs into two sub-populations depending on size (Poon et al., 2014). The device sorted up to 3 million cells per minute. Despite some overlap between the larger ($2r_c$ = 21.9 ± 5.3 μm) and smaller cell populations ($2r_c$ = 14.8 ± 2.4 μm), there was a correlation between the larger BMSCs and a commitment to osteoprogenitor lineages *in vitro*, as well as an increased survival of lethally irradiated mice after *in vivo* transplantation with the larger BMSC fraction. The same device was used to separate cells by exploiting size differences in disparate cell cycle phases (Lee et al., 2011). BMSC biophysical markers such as size, nuclear fluctuation and deformability have been related to the differentiation potency, associating smaller, softer and high nuclear fluctuation phenotypes with increased multipotency (Lee et al., 2014).

The group of Di Carlo demonstrated label-free separation of adrenal cortical progenitor cells from digestions of murine adrenal glands (Hur et al., 2012). The smaller progenitor cells were isolated from the larger somatic cells and large clusters through different magnitudes of inertial lift forces in a long rectangular channel. The progenitor cells were positioned nearest to the channel walls, and sorted at rates of 24,000 cells per minute, though purity and recovery rates are not reported.

In 2011, Bhagat *et al.* described a pinched-flow inertial microfluidic device for sorting MCF-7 cells spiked into diluted whole blood. Over 80% of the cells were recovered with a 5.5 and 4.1 log-depletion of RBCs and WBCs, respectively. However, the purity was only about 0.025% owing to the presence of large numbers of RBCs at the sample outlet (Bhagat et al., 2011). Later, Shen *et al.* combined inertial microfluidics with steric hindrance into a single system achieving a 5.3 log-depletion of all blood cells in a sample diluted 40 times and spiked with fewer than 1,000 CTCs/mL, which was comparable to the work of Bhagat *et al*. Recovery of 90% of the CTCs equated to a purity of 20% (Shen et al., 2014).

Finally two publications used spiral micro-channels (Fig. 5e) to sort CTCs spiked into diluted (Hou et al., 2013) or RBC-lysed whole blood (Warkiani et al., 2013). In the first example, 85% of CTCs were recovered, equivalent to a 9 and 3 log-depletion of RBCs and WBCs respectively, with purities of over 95% (Hou et al., 2013). In the second, Warkiani *et al.* introduced an RBC-lysis step and improved WBC depletion up to 4-log, resulting in a CTC purity of 80%, which is an improvement over the previous example since the CTC concentration was 5,000 times less (100 compared to 5 million) (Warkiani et al., 2013). Both publications also report the isolation and detection of CTCs from patients with metastatic lung and breast cancer. Detection was achieved in 20 out of 20 (Hou et al., 2013) and 10 out of 10 samples (Warkiani et al., 2013). A detailed protocol of Warkiani's device was published recently (Warkiani et al., 2016) showing a multiplexed version that increased the device recovery efficiency to 85% while retaining its high throughput (Warkiani et al., 2014).

Inertial microfluidic devices are typically associated with high flow rates, of the order of millilitres per minute, and throughputs of up to hundreds of millions of cells per minute. As previously discussed, this feature is invaluable for sorting rare cell populations. However, the reported purities are only as high as 80% for relatively rare cell populations (100 CTCs/mL RBC-lysed blood) (Warkiani et al., 2013). These values are low compared with the required purity for SSC applications. Consequently, inertial microfluidics for sorting SSCs from bone marrow would need to be improved, or again combined with another sorting technique, to deliver the required purity.

3.5. Acoustophoresis

The first reports of particle manipulation using ultrasonic sound waves date as far back as the early 1900's (King and Macdonald, 1934) but it was only recently that acoustic forces were used for on-chip continuous flow separation, combining small dimension devices with higher resonance frequency transducers to improve separation performance (Hawkes and Coakley, 2001; Laurell et al., 2007).

The principles of acoustophoresis lie in the generation of an acoustic standing wave between two sound sources, commonly a piezoceramic actuator facing a sound reflector. At a given frequency, half the wavelength of the ultrasound matches the width of the channel where the reflector is located and a standing wave is generated (Fig. 6a). Cells within this pressure wave experience acoustic radiation forces, provided that their acoustic properties differ from that of the medium. This force is given by the acoustic contrast factor Φ, which depends on both the densities (ρ_c and ρ_m) and the speed of sound (c_c and c_m) in the cell and the suspending medium: (Laurell et al., 2007; Lenshof et al., 2012; Lenshof and Laurell, 2011; Petersson et al., 2007)

$$\Phi = \frac{\rho_c + \frac{2}{3}(\rho_c - \rho_m)}{2\rho_c + \rho_m} - \frac{1}{3}\frac{\rho_m c_m^2}{\rho_c c_c^2} \quad (8)$$

These forces can be divided into the primary radiation force (Equation 9) generated from the standing wave, and the secondary Bjerknes forces, which arise from scattered waves due to particle-particle interaction (Gröschl, 1998). Secondary Bjerknes forces are inversely proportional to the distance between particles to the power of 4 and are therefore negligible in most applications (Kapishnikov et al., 2006; Laurell et al., 2007).

$$F_{acoustic} = 4\pi {r_c}^3 E_{ac} k \sin(2kz)\Phi \quad (9)$$

In equation 9, E_{ac} is the acoustic energy density, k the wavenumber ($2\pi f/c_m$), and z the distance between cell and pressure anti-node. From equations 8 and 9 it is evident that particle sorting through acoustophoresis can be achieved through differences in cell size (r_c), density (ρ_c) or compressibility, which relates directly to the speed of sound inside the cell (c_c).

(Please insert Figure 6 after this paragraph)

The sign of the acoustic contrast factor determines whether the cell is pushed towards a pressure node or anti-node (Kapishnikov et al., 2006; Laurell et al., 2007; Lenshof et al., 2012). Cells with opposing contrast factors can be separated by being concentrated in different locations inside the channel. Most commonly, acoustophoretic sorting is achieved using a single pressure node located at the centre of the channel (Lenshof and Laurell, 2011). Therefore, particles with positive factors (most solid particles and cells in aqueous conditions) are drawn to the centre of the channel, whereas particles with negative factors (air bubbles or oil droplets) are drawn to the pressure anti-nodes near the channel walls (Fig. 6b and c) (Lenshof and Laurell, 2011).

When cells have similar contrast factors, separation can be performed based on size. The acoustic force is directly proportional to the cell volume and therefore larger cells will be displaced faster than smaller cells so that they can be collected in different outlets (Fig. 6c). Reviews on the physics of acoustophoresis as well as potential applications can be found elsewhere (Kapishnikov et al., 2006; Laurell et al., 2007; Lenshof et al., 2012; Lenshof and Laurell, 2011).

Using acoustophoresis, spiked CTCs have been sorted from RBC-lysed whole blood obtained from healthy volunteers (Augustsson et al., 2012; Ding et al., 2014). Using tilted-angle standing surface acoustic waves, MCF-7, spiked at $3x10^5$ cells/mL, were sorted with 84% purity with a recovery of 71% of the cells (Ding et al., 2014). Augustsson *et al.* obtained higher purities when sorting prostate cancer cell lines. The best results were obtained with fixed cells. DU145 cells could be sorted with a purity of 98% and very little cell loss (3%). PC3 cells behaved similarly to DU145 but results with LNCaP cells were disappointing, with recovery rates lower than 80% and purity in the range of 60%. The authors speculate that differences in density and/or compressibility of these cells were responsible for the lower efficiency. For live unfixed cells the best results were obtained again with DU145 but with slightly lower purity (93%) and higher cell loss (16.3%). Recently, the same group demonstrated sorting of fixed DU145 from WBCs with similar results but using a single-inlet two-stage acoustophoresis device (Antfolk et al., 2015). The first stage pre-positions all cells near the walls of the device eliminating the need for sheath flow focusing. A second acoustophoretic stage, actuated at 2 MHz, draws all cells into the centre of the channel allowing kinetic separation of the larger CTCs in a central outlet (Fig. 6d). It should be noted that in all these applications, CTCs were spiked at concentrations of 10^4 to 10^5-fold higher than those found in clinical samples (Miller et al., 2009).

Regarding rare progenitor cells, Dykes et al. used acoustophoresis to deplete platelets from peripheral blood progenitor cell (PBPC) samples obtained by leukapheresis, ultimately for haematopoietic stem cell transplantation (Dykes et al., 2011). Platelets were depleted by 88% while almost 98% of the leukocytes were retained. The authors also demonstrated that the progenitor cells retained viability and maintained their colony-forming ability post-sorting. The same group used immunomagnetic beads to alter the acoustic properties of the cells to achieve improved separation (Lenshof et al., 2014). $CD4^+$ lymphocytes were separated from RBC-depleted PBPC samples with 87% purity and separation efficiencies of 65%, comparable to MACS. Cell viability was not affected and both the $CD4^+$ lymphocytes and the non-targeted progenitors function was preserved.

One aspect that stands out from all these applications is that in all cases separation was achieved based on differences in cell size. In the one case in which cell discrimination by size was not possible, $CD4^+$ lymphocytes needed to be immuno-labelled to alter their acoustic properties and allow separation (Lenshof et al., 2014). Sorting SSCs based on size differences is unlikely to discriminate sufficiently, as SSCs are characterised by a broad distribution in size and co-localise mainly with the monocyte population (Janeczek et al., 2015b). Additionally, antibody-labelling will not provide an improvement over current SSC sorting techniques while a specific SSC marker is yet to be identified. Most of the publications used samples which had been subjected to some kind of decomplexation and with a high concentration of targeted cells. Given the rarity of SSCs and the complexity of bone marrow tissue, none of these papers described a technology that would be suitable for SSC isolation. Finally, only one publication reports a high throughput (300,000 cells/min) (Lenshof et al., 2014), of the order of magnitude required for SSC isolation from a bone marrow buffy coat which can comprise up to a hundred million cells. Thus, acoustophoresis may not demonstrate the throughput required for sorting SSCs from bone marrow harvests. However, like DLD, acoustophoresis could be used for decomplexing, to enrich the SSCs in a bone marrow buffy coat through size fractionation. Further purification could be achieved in a two-stage acoustophoresis approach by immuno-labelling the remaining contaminant cells in order to change their acoustic contrast factor.

3.6. Dielectrophoresis (DEP)

When a biological particle is subjected to an electric field, it polarises due to the accumulation of charge at interfaces such as the cell membrane with the surrounding medium, leading to the formation of an induced electrical dipole (Gascoyne and Shim, 2014; Morgan and Green, 2003; Pethig, 2010; Pethig et al., 2010). Provided that the electrode geometry creates a non-homogeneous electric field, this polarisation gives rise to a force on the cell called dielectrophoresis (DEP). The cell can move towards or away from high field regions, termed positive (pDEP) or negative (nDEP) dielectrophoresis, respectively (Fig. 7a). The magnitude of the DEP force scales with cell volume and also with the electric field gradient which depends on the applied voltage and electrode geometry. The DEP force also depends on the cell's polarizability, which is frequency-dependent (Fig. 7b), and is given by: (Gascoyne and Shim, 2014; Morgan and Green, 2003; Pethig, 2010; Pethig et al., 2010)

$$F_{DEP} = 2\pi\varepsilon_m r_c^3 Re(f_{CM})\nabla|E|^2 \quad (10) \qquad with\ f_{CM} = \frac{\tilde{\varepsilon}_P - \tilde{\varepsilon}_m}{\tilde{\varepsilon}_P + 2\tilde{\varepsilon}_m} \quad (11)$$

In equation 10, ε_m is the absolute permittivity of the suspending medium, r_c is the cell radius, $\nabla|E|^2$ the gradient of the electric field squared, and $Re(f_{CM})$ the real part of the Clausius-Mossotti factor which reflects the cell's polarizability. The Clausius-Mossotti factor (Equation 11), depends on frequency, and on both the cell and the suspending medium complex permittivity, which is given by $\tilde{\varepsilon} = \varepsilon - j\sigma/\omega$, where j^2=-1, ω is the angular frequency and ε and σ the permittivity and conductivity, respectively. The subscripts "p" and "m" refer to particle and medium.

(Please insert Figure 7 after this paragraph)

For cell sorting, DEP separation is usually performed using a suspending medium with a low conductivity. At lower frequencies, cells experience negative DEP. At higher frequencies, cells experience positive DEP and are attracted to electrodes (Fig. 7a, b) (Gascoyne and Shim, 2014; Morgan and Green, 2003; Pethig, 2010; Pethig et al., 2010). The frequency at which this response changes from nDEP to pDEP is called the cross-over frequency (f_{xo}), and this depends primarily on the cell membrane capacitance (C_{mem}) and size: (Pethig et al., 2010)

$$f_{xo} = \frac{\sqrt{2}}{2\pi r_c C_{mem}} \quad (12)$$

Cell populations with different membrane capacitance, which reflects changes on for example the membrane's roughness, or size may therefore experience DEP forces of different magnitudes and/or directions so that they can be sorted. Fig. 7b shows a plot of the polarizability of three cell types with different sizes and membrane capacitance. Regions I and III represent frequency ranges in which all cells experience DEP forces with the same direction but with different magnitudes allowing for separation. Region II represents a frequency window in which cells experience DEP forces with opposite directions, allowing for selective DEP sorting. Many different strategies have been developed to sort cells by DEP, including focusing, trapping, or deflecting cells into different flow streams (Fig. 7c) (Cheng et al., 2007; Gagnon, 2011; Gascoyne and Vykoukal, 2002; Hughes, 2002; Khoshmanesh et al., 2011; Pethig, 2010).

An early paper describing DEP cell sorting used positive DEP to trap and enrich $CD34^+$ human HSCs in leukocyte fractions obtained from buffy coats of peripheral blood and bone marrow samples (Talary et al., 1995). However, the final purity was low (just under 5% $CD34^+$ cells) and the enrichment under 6-fold. Five years later, Wang *et al.* sorted $CD34^+$ HSCs (obtained by MACS separation of peripheral blood), from a human breast cancer cell line mixed 50:50 (Wang et al., 2000). At a high throughput ($1.2x10^5$ cells/min), the enrichment was almost 2-fold with a final purity of over 99% HSCs. The study included other separations such as the enrichment of leukocytes in diluted whole blood and the separation of different leukocyte populations. In this setup, a negative DEP force generated by electrodes on the bottom of a microfluidic channel levitated cells to different heights depending on their dielectric properties and buoyancy. This force pushes cells into different equilibrium positions and therefore different flow streams thus leading to kinetic separation under the influence of the parabolic flow profile, in a technique known as field flow fractionation (DEP-FFF) (Wang et al., 2000).

Flanagan *et al.* showed separation of astrogenic and neurogenic progenitors from neural progenitor/stem cell samples obtained from the cerebral cortex of mice brains. In their most recent publication (Simon et al., 2014), viable astrocyte progenitor-enriched populations were sorted by DEP at a rate of 2,500 cells per minute. In these devices, interdigitated electrode arrays in a microfluidic chamber were actuated with a 7 V_{p-p} signal at 1 MHz to trap all viable cells. Sequentially, under a constant buffer flow, the frequency was lowered in 100 kHz increments, releasing cells from the array according to their cross-over frequency. As the average cell size was the same for different fractions, separation was based on differences in the membrane capacitance of neuroprogenitors which was higher for astrogenic-committed than neurogenic-committed cells. The dielectric properties of astrocytes, neurons and their progenitors were characterised according to their DEP trapping over certain frequency ranges (Flanagan et al., 2008; Labeed et al., 2011; Lu et al., 2012).

Muratore *et al.* recently described negative DEP separation of myoblasts from their progeny after a 7-day differentiation protocol. Approximately 40 to 70% of the myoblasts differentiated into myotubes, which after separation yielded 95% and almost 99% pure populations of myoblasts and myotubes, respectively. However, the viability of the myotubes was reduced by the DEP separation protocol by more than 30%. In this work the authors suggested that separation was based on differences on the lipid composition of the cell membranes, verified by Raman spectroscopy, which might alter the membrane relative permittivity (Muratore et al., 2012).

Two publications demonstrate sorting of human BMSCs (Song et al., 2015; Vykoukal et al., 2008). In the first, a human immortalised MSC cell line was differentiated into osteoblasts. The two cell populations were separately harvested, mixed

together in a 1:1 ratio and processed at 300 cells per minute through a microfluidic chamber with oblique interdigitated electrodes. Osteoblasts experienced stronger positive DEP forces and were deflected laterally into a different outlet. Although sorting efficiencies were not high (86% and 67% recovery efficiencies, for MSCs and osteoblasts respectively), this work was an important proof of principle of sorting BMSCs using DEP (Song et al., 2015). Vykoukal *et al.* also used DEP-FFF to enrich populations of $NG2^+$ putative adipose-derived stromal stem cells from human samples (Vykoukal et al., 2008). A 14-fold enrichment was obtained, increasing the amount of $NG2^+$ cells from almost 2% to over 27%.

The MG-63 cell line is osteoblast-like and commonly used as a Stro-1^+ model for SSCs. Their dielectric properties were measured by DEP and compared to another osteosarcoma cell line, Saos-2, and human primary Stro-1^+ SSCs (Ismail et al., 2015). Ling *et al.* took advantage of the much larger size of MG-63 to sort them from erythrocytes by positive DEP using a periodic microelectrode array, obtaining a purity of 83% (11-fold enrichment) (Ling et al., 2012), though fractionation was not performed.

Throughput in DEP is generally very low, apart from the work of Wang *et al.* in which cells were sorted at over 100,000 per minute (Wang et al., 2000). Most separations shown above were performed on samples in which the target cells were not rare and with modest enrichment. Although this is true for all the applications shown with progenitor cells, examples with higher throughput and enrichment can be found in DEP approaches to CTC sorting. Moon *et al.* combined inertial microfluidics (an expansion and contraction array) with DEP to separate MCF-7 cells mixed with WBCs and RBCs in a 1 to 1 to 1,000 ratio (Moon et al., 2011). At the end of the two separation stages, up to 75% of the cancer cells were recovered with approximately 16% purity, representing a 160-fold enrichment. The total throughput was higher than 1 million cells per minute, although this was mostly due to the first inertial microfluidic separation. Shim *et al.* used a continuous flow DEP-FFF approach to sort tumour cells spiked at a low frequency (50-600/mL) into the buffy coats of healthy peripheral blood samples (Shim et al., 2013). The reported throughput was the highest achieved for DEP sorting, with up to a million cells per minute. Purities of 80% were achieved with a recovery of about 75% of the spiked tumour cells.

4. Future prospects on label-free sorting of human skeletal stem cells

Microfluidic techniques for stem cell sorting are at an early stage and with few publications. However, separation technologies exist and have been improved over the past few years, as evidenced by the progress in sorting CTCs from complex or even clinical samples. In sorting SSCs from the bone marrow, high purity is a significant concern with target values of 100% pure populations. MACS separation of Stro-1^+ cells provides a 950-fold enrichment of SSCs over bone marrow stromal cell populations (Gronthos et al., 2003), a value which can be further increased to 2,000-fold by further selection of $CD146^+$ cells (Shi and Gronthos, 2003). Such enrichment factors are far above the best examples using microfluidic techniques for sorting stem cells (Vykoukal et al., 2008), but are clearly in the range of enrichment values achieved for sorting CTCs from whole blood, which can reach 10^4-fold (Karabacak et al., 2014; Shen et al., 2014), or from relevant examples found for sorting progenitor cells, such as nucleated RBCs, in which over 10^3-fold enrichment was achieved (Huang et al., 2008). Table 3 summarises the best examples found for each technique.

Table 1 *– Summary of the best performance examples of the reviewed microfluidic label-free sorting techniques*

Technique	Discriminating features	Throughput	Purity	Enrichment	Recovery rate	Label-free
DLD	Size, shape, deformability	$1.8x10^9$ cells/min (D'Silva et al., 2015)	98.7% (Liu et al., 2013)	Total removal of platelets and RBCs (Karabacak et al., 2014; Ozkumur et al., 2013) 174-fold (D'Silva et al., 2015)	99% (Liu et al., 2013)	Yes
Acoustophoresis	Size, density, compressibility	$3x10^5$ cells/min (Lenshof et al., 2014)	98% (Augustsson et al., 2012)	8.4-fold (Ding et al., 2014)	98% (Dykes et al., 2011)	Yes
Inertial microfluidics	Size, deformability, density	$2.5x10^8$ cells/min (Hou et al., 2013)	99% (Didar et al., 2013)	10^9-fold (over RBCs) (Hou et al., 2013) $10^{3.3}$-fold (over WBCs) (Hou et al., 2013)	99.1% (Lee et al., 2013)	Yes
Dielectrophoresis	Size, dielectric properties	$1.25x10^6$ cells/min (Moon et al., 2011)	99% (Wang et al., 2000)	10^4-fold (Shim et al., 2013)	92% (Gascoyne et al., 2009)	Yes
Magnetophoresis	Magnetic susceptibility, Antibody-labelling	$4x10^6$ cells/min (Chung et al., 2013)	50% (Ozkumur et al., 2013)	$10^{3.8}$-fold (Ozkumur et al., 2013)	97% (Karabacak et al., 2014)	Yes, if used for negative-depletion
Affinity-based	Antibody-labelling	$1x10^8$ cells/min (Stott et al., 2010a)	68% (Gleghorn et al., 2010)	~10^9-fold (Gleghorn et al., 2010; Nagrath et al., 2007; Stott et al., 2010a)	92% (Stott et al., 2010a)	No

Given the rarity of SSCs in human bone marrow (1 in 100,000), a high throughput separation method is critical to enable a practical number of cells to be sorted for clinical applications. Ideally, a throughput of around one million cells per minute would be desirable for sorting bone marrow buffy coat, or even higher for sorting non-processed bone marrow. With the exception of acoustophoresis and possibly DEP, most microfluidic sorting techniques have now demonstrated very high throughput in the range of millions of cells per minute (Table 1), which should be adequate for sorting SSCs. Sorting SSCs from human bone marrow with high purity and within a reasonable amount of time, will likely require a combination of different sorting techniques rather than one single technique. For example a decomplexing step based on cell size fractionation followed by a refining step to increase final purity.

Label free separation approaches will depend on identifying unique biophysical features of SSCs that make them distinct and distinguishable from other cells in the bone marrow. High-throughput single-cell characterisation techniques like microfluidic impedance cytometry (Sun and Morgan, 2010) and real-time deformability cytometry (RT-DC) (Otto et al., 2015) can provide data on cell dielectric and elastic properties. Using RT-DC it has recently been shown, that enriched SSC populations, are significantly stiffer than cells from the haematopoietic lineage found in the bone marrow, namely, lymphocytes, monocytes, granulocytes and a blood progenitor cell line, HL-60, which are commonly used as a model for HSCs (Xavier et al., 2016). Such differences could be exploited for separation using for example DLD, which is sensitive to differences in cells deformability (Beech et al., 2012; Holmes et al., 2014).

Fig. 8 shows a possible four-step strategy for sorting SSCs. The first step performs successive washes and separation of the marrow sample to remove fat, bone debris and the larger megakaryocytes. A second step based on either a density centrifugation or selective lysis depletes the RBCs. Cell lysis is advantageous in terms of rapid processing and simplicity. Density centrifugation, however, is slower and is less than 100% effective, but it is able to partially deplete the sample of contaminating platelets and granulocytes. Subsequent purification steps might involve DLD separation, for example to remove cells smaller than a critical size. In this context, estimates of the SSC size (Fig. 8) are made from adherent cells under expansion. Designing a DLD device requires knowledge of the size of SSCs in freshly harvested samples. Finally, it should be noted that while these approaches will significantly enhance SSC enrichment, the application of DLD to reduce cell numbers and fractionate by cell size would still leave a sample that is significantly contaminated by cells that are similar in size to the SSC. One approach to further improve SSC enrichment would be the application of magnetophoresis for negative depletion of all contaminant cells targeting markers not expressed by SSCs. This would negate the issues surrounding the use of positive selection of SSCs given the poor specificity of current markers. Whilst these proposed approaches are not trivial, microfluidic techniques could provide innovative solutions for sorting skeletal stem cells from human bone marrow with significant physiological and therapeutic implications.

(Please insert Figure 8 after this paragraph)

5. Acknowledgements

This work was supported by the European Commission through the Label-free particle sorting (LAPASO) project from the People Programme (Marie Curie Actions) of the European Union's Seventh Framework Programme FP7/2007-2013 under REA grant agreement n° 607350.

6. References

Alt, E., Yan, Y., Gehmert, S., Song, Y.-H., Altman, A., Gehmert, S., Vykoukal, D., Bai, X., 2011. Fibroblasts share mesenchymal phenotypes with stem cells, but lack their differentiation and colony-forming potential. Biol. Cell Auspices Eur. Cell Biol. Organ. 103, 197–208. doi:10.1042/BC20100117

Amini, H., Lee, W., Carlo, D.D., 2014. Inertial microfluidic physics. Lab. Chip 14, 2739–2761. doi:10.1039/C4LC00128A

Antfolk, M., Antfolk, C., Lilja, H., Laurell, T., Augustsson, P., 2015. A single inlet two-stage acoustophoresis chip enabling tumor cell enrichment from white blood cells. Lab. Chip 15, 2102–2109. doi:10.1039/C5LC00078E

Augustsson, P., Magnusson, C., Nordin, M., Lilja, H., Laurell, T., 2012. Microfluidic, Label-Free Enrichment of Prostate Cancer Cells in Blood Based on Acoustophoresis. Anal. Chem. 84, 7954–7962. doi:10.1021/ac301723s

Beech, J.P., Holm, S.H., Adolfsson, K., Tegenfeldt, J.O., 2012. Sorting cells by size, shape and deformability. Lab. Chip 12, 1048. doi:10.1039/c2lc21083e

Beech, J.P., Jönsson, P., Tegenfeldt, J.O., 2009. Tipping the balance of deterministic lateral displacement devices using dielectrophoresis. Lab. Chip 9, 2698–2706. doi:10.1039/B823275J

Bhagat, A.A.S., Hou, H.W., Li, L.D., Lim, C.T., Han, J., 2011. Pinched flow coupled shear-modulated inertial microfluidics for high-throughput rare blood cell separation. Lab. Chip 11, 1870–1878. doi:10.1039/C0LC00633E

Bianco, P., 2015. Stem cells and bone: A historical perspective. Bone 70C, 2–9. doi:10.1016/j.bone.2014.08.011

Bianco, P., Cao, X., Frenette, P.S., Mao, J.J., Robey, P.G., Simmons, P.J., Wang, C.-Y., 2013. The meaning, the sense and the significance: translating the science of mesenchymal stem cells into medicine. Nat. Med. 19, 35–42. doi:10.1038/nm.3028

Bianco, P., Robey, P.G., 2015. Skeletal stem cells. Development 142, 1023–1027. doi:10.1242/dev.102210

Bonner, W.A., Hulett, H.R., Sweet, R.G., Herzenberg, L.A., 1972. Fluorescence Activated Cell Sorting. Rev. Sci. Instrum. 43, 404–409. doi:10.1063/1.1685647

Carlo, D.D., 2009. Inertial microfluidics. Lab. Chip 9, 3038–3046. doi:10.1039/B912547G

Carlo, D.D., Irimia, D., Tompkins, R.G., Toner, M., 2007. Continuous inertial focusing, ordering, and separation of particles in microchannels. Proc. Natl. Acad. Sci. 104, 18892–18897. doi:10.1073/pnas.0704958104

Chasis, J.A., Mohandas, N., 1992. Red blood cell glycophorins. Blood 80, 1869–1879.

Chauhan, H., Abraham, A., Phillips, J.R.A., Pringle, J.H., Walker, R.A., Jones, J.L., 2003. There is more than one kind of myofibroblast: analysis of CD34 expression in benign, in situ, and invasive breast lesions. J. Clin. Pathol. 56, 271–276. doi:10.1136/jcp.56.4.271

Cheng, I.-F., Chang, H.-C., Hou, D., Chang, H.-C., 2007. An integrated dielectrophoretic chip for continuous bioparticle filtering, focusing, sorting, trapping, and detecting. Biomicrofluidics 1, 021503. doi:10.1063/1.2723669

Chen, Y., Li, P., Huang, P.-H., Xie, Y., Mai, J.D., Wang, L., Nguyen, N.-T., Huang, T.J., 2014. Rare cell isolation and analysis in microfluidics. Lab. Chip 14, 626–645. doi:10.1039/C3LC90136J

Christensen, K., Doblhammer, G., Rau, R., Vaupel, J.W., 2009. Ageing populations: the challenges ahead. The Lancet 374, 1196–1208. doi:10.1016/S0140-6736(09)61460-4

Christenson, L.K., Stouffer, R.L., 1996. Isolation and culture of microvascular endothelial cells from the primate corpus luteum. Biol. Reprod. 55, 1397–1404. doi:10.1095/biolreprod55.6.1397

Chung, J., Issadore, D., Ullal, A., Lee, K., Weissleder, R., Lee, H., 2013. Rare cell isolation and profiling on a hybrid magnetic/size-sorting chip. Biomicrofluidics 7, 054107. doi:10.1063/1.4821923

Collins, D.J., Alan, T., Neild, A., 2014. Particle separation using virtual deterministic lateral displacement (vDLD). Lab. Chip 14, 1595–1603. doi:10.1039/C3LC51367J

Dawson, J.I., Kanczler, J., Tare, R., Kassem, M., Oreffo, R.O.C., 2014. Concise Review: Bridging the Gap: Bone Regeneration Using Skeletal Stem Cell-Based Strategies—Where Are We Now? STEM CELLS 32, 35–44. doi:10.1002/stem.1559

Devendra, R., Drazer, G., 2012. Gravity Driven Deterministic Lateral Displacement for Particle Separation in Microfluidic Devices. Anal. Chem. 84, 10621–10627. doi:10.1021/ac302074b

Di Carlo, D., Edd, J.F., Humphry, K.J., Stone, H.A., Toner, M., 2009. Particle Segregation and Dynamics in Confined Flows. Phys. Rev. Lett. 102, 094503. doi:10.1103/PhysRevLett.102.094503

Didar, T.F., Li, K., Veres, T., Tabrizian, M., 2013. Separation of rare oligodendrocyte progenitor cells from brain using a high-throughput multilayer thermoplastic-based microfluidic device. Biomaterials 34, 5588–5593. doi:10.1016/j.biomaterials.2013.04.014

Ding, X., Peng, Z., Lin, S.-C.S., Geri, M., Li, S., Li, P., Chen, Y., Dao, M., Suresh, S., Huang, T.J., 2014. Cell separation using tilted-angle standing surface acoustic waves. Proc. Natl. Acad. Sci. 111, 12992–12997. doi:10.1073/pnas.1413325111

D'Silva, J., Austin, R., Sturm, J.C., 2015. Inhibition of Clot Formation in Deterministic Lateral Displacement Arrays for Processing Large Volumes of Blood for Rare Cell Capture. Lab. Chip. doi:10.1039/C4LC01409J

Dykes, J., Lenshof, A., Åstrand-Grundström, I.-B., Laurell, T., Scheding, S., 2011. Efficient Removal of Platelets from Peripheral Blood Progenitor Cell Products Using a Novel Micro-Chip Based Acoustophoretic Platform. PLoS ONE 6. doi:10.1371/journal.pone.0023074

Fåhræus, R., Lindqvist, T., 1931. The Viscosity of the Blood in Narrow Capillary Tubes. Am. J. Physiol. -- Leg. Content 96, 562–568.

Fawcett, D., Bloom, W., 1994. Bone Marrow and Blood Cell Formation, in: A Textbook of Histology. Chapman & Hall.

Flanagan, L.A., Lu, J., Wang, L., Marchenko, S.A., Jeon, N.L., Lee, A.P., Monuki, E.S., 2008. Unique Dielectric Properties Distinguish Stem Cells and Their Differentiated Progeny. STEM CELLS 26, 656–665. doi:10.1634/stemcells.2007-0810

Freitas, R.A., 2003. Nanomedicine. S. Karger AG.

Friedenstein, A.J., Owen, M., 1988. Stromal Stem Cells: Marrow-derived osteogenic precursors, in: Cell and Molecular Biology of Vertebrate Hard Tissues. CIBA Foundation Symposium, p. 321.

Friedenstein, A.J., Petrakova, K.V., Kurolesova, A.I., Frolova, G.P., 1968. HETEROTOPIC TRANSPLANTS OF BONE MARROW. Transplantation 6, 230–247.

Friedenstein, A.J., Piatetzky-Shapiro, I.I., Petrakova, K.V., 1966. Osteogenesis in transplants of bone marrow cells. J. Embryol. Exp. Morphol. 16, 381–390.

Gagnon, Z.R., 2011. Cellular dielectrophoresis: Applications to the characterization, manipulation, separation and patterning of cells. ELECTROPHORESIS 32, 2466–2487. doi:10.1002/elps.201100060

Galletti, G., Sung, M.S., Vahdat, L.T., Shah, M.A., Santana, S.M., Altavilla, G., Kirby, B.J., Giannakakou, P., 2013. Isolation of breast cancer and gastric cancer circulating tumor cells by use of an anti HER2-based microfluidic device. Lab. Chip 14, 147–156. doi:10.1039/C3LC51039E

Gascoyne, P.R.C., Noshari, J., Anderson, T.J., Becker, F.F., 2009. Isolation of rare cells from cell mixtures by dielectrophoresis. ELECTROPHORESIS 30, 1388–1398. doi:10.1002/elps.200800373

Gascoyne, P.R.C., Shim, S., 2014. Isolation of Circulating Tumor Cells by Dielectrophoresis. Cancers 6, 545–579. doi:10.3390/cancers6010545

Gascoyne, P.R.C., Vykoukal, J., 2002. Particle separation by dielectrophoresis. ELECTROPHORESIS 23, 1973–1983. doi:10.1002/1522-2683(200207)23:13<1973::AID-ELPS1973>3.0.CO;2-1

Geislinger, T.M., Franke, T., 2014. Hydrodynamic lift of vesicles and red blood cells in flow — from Fåhræus & Lindqvist to microfluidic cell sorting. Adv. Colloid Interface Sci., Special issue in honour of Wolfgang Helfrich 208, 161–176. doi:10.1016/j.cis.2014.03.002

Gleghorn, J.P., Pratt, E.D., Denning, D., Liu, H., Bander, N.H., Tagawa, S.T., Nanus, D.M., Giannakakou, P.A., Kirby, B.J., 2010. Capture of circulating tumor cells from whole blood of prostate cancer patients using geometrically enhanced differential immunocapture (GEDI) and a prostate-specific antibody. Lab. Chip 10, 27–29. doi:10.1039/B917959C

Gossett, D.R., Weaver, W.M., Mach, A.J., Hur, S.C., Tse, H.T.K., Lee, W., Amini, H., Di Carlo, D., 2010. Label-free cell separation and sorting in microfluidic systems. Anal. Bioanal. Chem. 397, 3249–3267. doi:10.1007/s00216-010-3721-9

Gothard, D., Dawson, J.I., Oreffo, R.O.C., 2013. Assessing the potential of colony morphology for dissecting the CFU-F population from human bone marrow stromal cells. Cell Tissue Res. 352, 237–247. doi:10.1007/s00441-013-1564-3

Gothard, D., Greenhough, J., Ralph, E., Oreffo, R.O., 2014. Prospective isolation of human bone marrow stromal cell subsets: A comparative study between Stro-1-, CD146- and CD105-enriched populations. J. Tissue Eng. 5, 2041731414551763. doi:10.1177/2041731414551763

Gothard, D., Tare, R.S., Mitchell, P.D., Dawson, J.I., Oreffo, R.O.C., 2011. In search of the skeletal stem cell: isolation and separation strategies at the macro/micro scale for skeletal regeneration. Lab. Chip 11, 1206–1220. doi:10.1039/c0lc00575d

Green, J.V., Radisic, M., Murthy, S.K., 2009. Deterministic Lateral Displacement as a Means to Enrich Large Cells for Tissue Engineering. Anal. Chem. 81, 9178–9182. doi:10.1021/ac9018395

Gronthos, S., Zannettino, A.C.W., Hay, S.J., Shi, S., Graves, S.E., Kortesidis, A., Simmons, P.J., 2003. Molecular and cellular characterisation of highly purified stromal stem cells derived from human bone marrow. J. Cell Sci. 116, 1827–1835. doi:10.1242/jcs.00369

Gröschl, M., 1998. Ultrasonic Separation of Suspended Particles - Part I: Fundamentals. Acta Acust. United Acust. 84, 432–447.

Halfon, S., Abramov, N., Grinblat, B., Ginis, I., 2010. Markers Distinguishing Mesenchymal Stem Cells from Fibroblasts Are Downregulated with Passaging. Stem Cells Dev. 20, 53–66. doi:10.1089/scd.2010.0040

Han, K.-H., Frazier, A.B., 2006. Paramagnetic capture mode magnetophoretic microseparator for high efficiency blood cell separations. Lab. Chip 6, 265–273. doi:10.1039/B514539B

Hawkes, J.J., Coakley, W.T., 2001. Force field particle filter, combining ultrasound standing waves and laminar flow. Sens. Actuators B Chem. 75, 213–222. doi:10.1016/S0925-4005(01)00553-6

Holmes, D., Whyte, G., Bailey, J., Vergara-Irigaray, N., Ekpenyong, A., Guck, J., Duke, T., 2014. Separation of blood cells with differing deformability using deterministic lateral displacement. Interface Focus 4, 20140011. doi:10.1098/rsfs.2014.0011

Holm, S.H., Beech, J.P., Barrett, M.P., Tegenfeldt, J.O., 2011. Separation of parasites from human blood using deterministic lateral displacement. Lab. Chip 11, 1326–1332. doi:10.1039/C0LC00560F

Holm, S.H., Beech, J.P., Tegenfeldt, J.O., 2013. Combined Density and Size-based Sorting in Deterministic Lateral Displacement Devices. Presented at the 17th International Conference on Miniaturized Systems for Chemistry and Life Sciences, 17th International Conference on Miniaturized Systems for Chemistry and Life Sciences.

Hou, H.W., Warkiani, M.E., Khoo, B.L., Li, Z.R., Soo, R.A., Tan, D.S.-W., Lim, W.-T., Han, J., Bhagat, A.A.S., Lim, C.T., 2013. Isolation and retrieval of circulating tumor cells using centrifugal forces. Sci. Rep. 3. doi:10.1038/srep01259

Huang, C., Liu, H., Bander, N.H., Kirby, B.J., 2013. Enrichment of prostate cancer cells from blood cells with a hybrid dielectrophoresis and immunocapture microfluidic system. Biomed. Microdevices 15, 941–948. doi:10.1007/s10544-013-9784-6

Huang, L.R., Cox, E.C., Austin, R.H., Sturm, J.C., 2004. Continuous Particle Separation Through Deterministic Lateral Displacement. Science 304, 987–990. doi:10.1126/science.1094567

Huang, R., Barber, T.A., Schmidt, M.A., Tompkins, R.G., Toner, M., Bianchi, D.W., Kapur, R., Flejter, W.L., 2008. A microfluidics approach for the isolation of nucleated red blood cells (NRBCs) from the peripheral blood of pregnant women. Prenat. Diagn. 28, 892–899. doi:10.1002/pd.2079

Huang, Y., Hoshino, K., Chen, P., Wu, C., Lane, N., Huebschman, M., Liu, H., Sokolov, K., Uhr, J.W., Frenkel, E.P., Zhang, J.X.J., 2012. Immunomagnetic nanoscreening of circulating tumor cells with a motion controlled microfluidic system. Biomed. Microdevices 15, 673–681. doi:10.1007/s10544-012-9718-8

Hughes, M.P., 2002. Strategies for dielectrophoretic separation in laboratory-on-a-chip systems. ELECTROPHORESIS 23, 2569–2582. doi:10.1002/1522-2683(200208)23:16<2569::AID-ELPS2569>3.0.CO;2-M

Hur, S.C., Brinckerhoff, T.Z., Walthers, C.M., Dunn, J.C.Y., Di Carlo, D., 2012. Label-Free Enrichment of Adrenal Cortical Progenitor Cells Using Inertial Microfluidics. PLoS ONE 7. doi:10.1371/journal.pone.0046550

Inglis, D.W., Lord, M., Nordon, R.E., 2011. Scaling deterministic lateral displacement arrays for high throughput and dilution-free enrichment of leukocytes. J. Micromechanics Microengineering 21, 054024. doi:10.1088/0960-1317/21/5/054024

Ismail, A., Hughes, M., Mulhall, H., Oreffo, R., Labeed, F., 2015. Characterization of human skeletal stem and bone cell populations using dielectrophoresis. J. Tissue Eng. Regen. Med. 9, 162–168. doi:10.1002/term.1629

Janeczek, A.A., Scarpa, E., Newman, T.A., Oreffo, R.O.C., Tare, R.S., Evans, N.D., 2015a. Skeletal Stem Cell Niche of the Bone Marrow, in: Turksen, K. (Ed.), Tissue-Specific Stem Cell Niche, Stem Cell Biology and Regenerative Medicine. Springer International Publishing, pp. 245–279.

Janeczek, A.A., Tare, R.S., Scarpa, E., Moreno-Jimenez, I., Rowland, C.A., Jenner, D., Newman, T.A., Oreffo, R.O.C., Evans, N.D., 2015b. Transient Canonical Wnt Stimulation Enriches Human Bone Marrow Mononuclear Cell Isolates for Osteoprogenitors. STEM CELLS n/a–n/a. doi:10.1002/stem.2241

Jing, Y., Moore, L.R., Schneider, T., Williams, P.S., Chalmers, J.J., Farag, S.S., Bolwell, B., Zborowski, M., 2007. Negative selection of hematopoietic progenitor cells by continuous magnetophoresis. Exp. Hematol. 35, 662–672. doi:10.1016/j.exphem.2006.12.009

Jones, E., McGonagle, D., 2008. Human bone marrow mesenchymal stem cells in vivo. Rheumatology 47, 126–131. doi:10.1093/rheumatology/kem206

Junqueira, L.C., Carneiro, J., 2005. Hematopoiesis, in: Basic Histology: Text and Atlas. McGraw Hill.

Kapishnikov, S., Kantsler, V., Steinberg, V., 2006. Continuous particle size separation and size sorting using ultrasound in a microchannel. J. Stat. Mech. Theory Exp. 2006, P01012. doi:10.1088/1742-5468/2006/01/P01012

Karabacak, N.M., Spuhler, P.S., Fachin, F., Lim, E.J., Pai, V., Ozkumur, E., Martel, J.M., Kojic, N., Smith, K., Chen, P., Yang, J., Hwang, H., Morgan, B., Trautwein, J., Barber, T.A., Stott, S.L., Maheswaran, S., Kapur, R., Haber, D.A., Toner, M., 2014. Microfluidic, marker-free isolation of circulating tumor cells from blood samples. Nat. Protoc. 9, 694–710. doi:10.1038/nprot.2014.044

Khoshmanesh, K., Nahavandi, S., Baratchi, S., Mitchell, A., Kalantar-zadeh, K., 2011. Dielectrophoretic platforms for bio-microfluidic systems. Biosens. Bioelectron. 26, 1800–1814. doi:10.1016/j.bios.2010.09.022

Kierszenbaum, A.L., Tres, L., 2015. Histology and Cell Biology: An Introduction to Pathology. Elsevier Health Sciences.

King, L., Macdonald, F., 1934. On the Acoustic Radiation Pressure on Spheres. Proc. R. Soc. London A147, 212–240.

Kirby, B.J., Jodari, M., Loftus, M.S., Gakhar, G., Pratt, E.D., Chanel-Vos, C., Gleghorn, J.P., Santana, S.M., Liu, H., Smith, J.P., Navarro, V.N., Tagawa, S.T., Bander, N.H., Nanus, D.M., Giannakakou, P., 2012. Functional Characterization of Circulating Tumor Cells with a Prostate-Cancer-Specific Microfluidic Device. PLoS ONE 7. doi:10.1371/journal.pone.0035976

Kolf, C.M., Cho, E., Tuan, R.S., 2007. Mesenchymal stromal cells. Biology of adult mesenchymal stem cells: regulation of niche, self-renewal and differentiation. Arthritis Res. Ther. 9, 204. doi:10.1186/ar2116

Kundrotas, G., 2012. Surface markers distinguishing mesenchymal stem cells from fibroblasts. MEZENCHIMINES KAMIENINES LASTELES NUO FIBROBLASTU ATSKIRIANTYS PAVIRŠIAUS ŽYMENYS 19, 75–79.

Kuntaegowdanahalli, S.S., Bhagat, A.A.S., Kumar, G., Papautsky, I., 2009. Inertial microfluidics for continuous particle separation in spiral microchannels. Lab. Chip 9, 2973–2980. doi:10.1039/B908271A

Labeed, F.H., Lu, J., Mulhall, H.J., Marchenko, S.A., Hoettges, K.F., Estrada, L.C., Lee, A.P., Hughes, M.P., Flanagan, L.A., 2011. Biophysical Characteristics Reveal Neural Stem Cell Differentiation Potential. PLoS ONE 6. doi:10.1371/journal.pone.0025458

Lara, O., Tong, X., Zborowski, M., Chalmers, J.J., 2004. Enrichment of rare cancer cells through depletion of normal cells using density and flow-through, immunomagnetic cell separation. Exp. Hematol. 32, 891–904. doi:10.1016/j.exphem.2004.07.007

Laurell, T., Petersson, F., Nilsson, A., 2007. Chip integrated strategies for acoustic separation and manipulation of cells and particles. Chem. Soc. Rev. 36, 492–506. doi:10.1039/B601326K

Lee, M.G., Shin, J.H., Bae, C.Y., Choi, S., Park, J.-K., 2013. Label-Free Cancer Cell Separation from Human Whole Blood Using Inertial Microfluidics at Low Shear Stress. Anal. Chem. 85, 6213–6218. doi:10.1021/ac4006149

Lee, W.C., Bhagat, A.A.S., Huang, S., Vliet, K.J.V., Han, J., Lim, C.T., 2011. High-throughput cell cycle synchronization using inertial forces in spiral microchannels. Lab. Chip 11, 1359–1367. doi:10.1039/C0LC00579G

Lee, W.C., Shi, H., Poon, Z., Nyan, L.M., Kaushik, T., Shivashankar, G.V., Chan, J.K.Y., Lim, C.T., Han, J., Vliet, K.J.V., 2014. Multivariate biophysical markers predictive of mesenchymal stromal cell multipotency. Proc. Natl. Acad. Sci. 111, E4409–E4418. doi:10.1073/pnas.1402306111

Lenshof, A., Jamal, A., Dykes, J., Urbansky, A., Åstrand-Grundström, I., Laurell, T., Scheding, S., 2014. Efficient purification of CD4+ lymphocytes from peripheral blood progenitor cell products using affinity bead acoustophoresis. Cytometry A 85, 933–941. doi:10.1002/cyto.a.22507

Lenshof, A., Laurell, T., 2011. Emerging Clinical Applications of Microchip-Based Acoustophoresis. J. Assoc. Lab. Autom. 16, 443–449. doi:10.1016/j.jala.2011.07.004

Lenshof, A., Magnusson, C., Laurell, T., 2012. Acoustofluidics 8: Applications of acoustophoresis in continuous flow microsystems. Lab. Chip 12, 1210–1223. doi:10.1039/C2LC21256K

Lin, G., Liu, G., Banie, L., Wang, G., Ning, H., Lue, T.F., Lin, C.-S., 2011. Tissue Distribution of Mesenchymal Stem Cell Marker Stro-1. Stem Cells Dev. 20, 1747–1752. doi:10.1089/scd.2010.0564

Ling, S.H., Lam, Y.C., Chian, K.S., 2012. Continuous Cell Separation Using Dielectrophoresis through Asymmetric and Periodic Microelectrode Array. Anal. Chem. 84, 6463–6470. doi:10.1021/ac300079q

Liu, Z., Huang, F., Du, J., Shu, W., Feng, H., Xu, X., Chen, Y., 2013. Rapid isolation of cancer cells using microfluidic deterministic lateral displacement structure. Biomicrofluidics 7, 011801. doi:10.1063/1.4774308

Lo Surdo, J., Bauer, S.R., 2012. Quantitative Approaches to Detect Donor and Passage Differences in Adipogenic Potential and Clonogenicity in Human Bone Marrow-Derived Mesenchymal Stem Cells. Tissue Eng. Part C Methods 18, 877–889. doi:10.1089/ten.tec.2011.0736

Loutherback, K., D'Silva, J., Liu, L., Wu, A., Austin, R.H., Sturm, J.C., 2012. Deterministic separation of cancer cells from blood at 10 mL/min. AIP Adv. 2, 042107. doi:10.1063/1.4758131

Lu, J., Barrios, C.A., Dickson, A.R., Nourse, J.L., Lee, A.P., Flanagan, L.A., 2012. Advancing practical usage of microtechnology: a study of the functional consequences of dielectrophoresis on neural stem cells. Integr. Biol. 4, 1223–1236. doi:10.1039/C2IB20171B

Lv, F.-J., Tuan, R.S., Cheung, K.M.C., Leung, V.Y.L., 2014. Concise Review: The Surface Markers and Identity of Human Mesenchymal Stem Cells. STEM CELLS 32, 1408–1419. doi:10.1002/stem.1681

Maheswaran, S., Sequist, L.V., Nagrath, S., Ulkus, L., Brannigan, B., Collura, C.V., Inserra, E., Diederichs, S., Iafrate, A.J., Bell, D.W., Digumarthy, S., Muzikansky, A., Irimia, D., Settleman, J., Tompkins, R.G., Lynch, T.J., Toner, M., Haber, D.A., 2008. Detection of Mutations in EGFR in Circulating Lung-Cancer Cells. N. Engl. J. Med. 359, 366–377. doi:10.1056/NEJMoa0800668

Martel, J.M., Toner, M., 2013. Particle Focusing in Curved Microfluidic Channels. Sci. Rep. 3. doi:10.1038/srep03340

May, J.A., Heptinstal, S., Fox, S.C., 2011. Stabilisation of blood cell conjugates. US20110059475 A1.

McGrath, J., Jimenez, M., Bridle, H., 2014. Deterministic lateral displacement for particle separation: a review. Lab. Chip 14, 4139–4158. doi:10.1039/C4LC00939H

Miller, M.C., Doyle, G.V., Terstappen, L.W.M.M., 2009. Significance of Circulating Tumor Cells Detected by the CellSearch System in Patients with Metastatic Breast Colorectal and Prostate Cancer. J. Oncol. 2010, e617421. doi:10.1155/2010/617421

Miltenyi, S., Müller, W., Weichel, W., Radbruch, A., 1990. High gradient magnetic cell separation with MACS. Cytometry 11, 231–238. doi:10.1002/cyto.990110203

Miyamoto, D.T., Lee, R.J., Stott, S.L., Ting, D.T., Wittner, B.S., Ulman, M., Smas, M.E., Lord, J.B., Brannigan, B.W., Trautwein, J., Bander, N.H., Wu, C.-L., Sequist, L.V., Smith, M.R., Ramaswamy, S., Toner, M., Maheswaran, S., Haber, D.A., 2012. Androgen Receptor Signaling in Circulating Tumor Cells as a Marker of Hormonally Responsive Prostate Cancer. Cancer Discov. 2, 995–1003. doi:10.1158/2159-8290.CD-12-0222

Moon, H.-S., Kwon, K., Kim, S.-I., Han, H., Sohn, J., Lee, S., Jung, H.-I., 2011. Continuous separation of breast cancer cells from blood samples using multi-orifice flow fractionation (MOFF) and dielectrophoresis (DEP). Lab. Chip 11, 1118–1125. doi:10.1039/C0LC00345J

Moore, L.R., Nehl, F., Dorn, J., Chalmers, J.J., Zborowski, M., 2013. Open Gradient Magnetic Red Blood Cell Sorter Evaluation on Model Cell Mixtures. IEEE Trans. Magn. 49, 309–315. doi:10.1109/TMAG.2012.2225098

Morgan, H., Green, N.G., 2003. AC electrokinetics: colloids and nanoparticles [WWW Document]. URL http://eprints.gla.ac.uk/33024/ (accessed 5.6.15).

Morton, K.J., Loutherback, K., Inglis, D.W., Tsui, O.K., Sturm, J.C., Chou, S.Y., Austin, R.H., 2008. Crossing microfluidic streamlines to lyse, label and wash cells. Lab. Chip 8, 1448–1453. doi:10.1039/B805614E

Muratore, M., Srsen, V., Waterfall, M., Downes, A., Pethig, R., 2012. Biomarker-free dielectrophoretic sorting of differentiating myoblast multipotent progenitor cells and their membrane analysis by Raman spectroscopy. Biomicrofluidics 6, 034113. doi:10.1063/1.4746252

Nagrath, S., Sequist, L.V., Maheswaran, S., Bell, D.W., Irimia, D., Ulkus, L., Smith, M.R., Kwak, E.L., Digumarthy, S., Muzikansky, A., Ryan, P., Balis, U.J., Tompkins, R.G., Haber, D.A., Toner, M., 2007. Isolation of rare circulating tumour cells in cancer patients by microchip technology. Nature 450, 1235–1239. doi:10.1038/nature06385

Otto, O., Rosendahl, P., Mietke, A., Golfier, S., Herold, C., Klaue, D., Girardo, S., Pagliara, S., Ekpenyong, A., Jacobi, A., Wobus, M., Töpfner, N., Keyser, U.F., Mansfeld, J., Fischer-Friedrich, E., Guck, J., 2015. Real-time deformability cytometry: on-the-fly cell mechanical phenotyping. Nat. Methods 12, 199–202. doi:10.1038/nmeth.3281

Ovalle, W.K., Nahirney, P.C., 2013. Netter's Essential Histology. Elsevier Health Sciences.

Owen, J.A., Punt, J., Kuby, J., Stranford, S.A., 2013. Kuby Immunology. W.H. Freeman.

Ozkumur, E., Shah, A.M., Ciciliano, J.C., Emmink, B.L., Miyamoto, D.T., Brachtel, E., Yu, M., Chen, P., Morgan, B., Trautwein, J., Kimura, A., Sengupta, S., Stott, S.L., Karabacak, N.M., Barber, T.A., Walsh, J.R., Smith, K., Spuhler, P.S., Sullivan, J.P., Lee, R.J., Ting, D.T., Luo, X., Shaw, A.T., Bardia, A., Sequist, L.V., Louis, D.N., Maheswaran, S., Kapur, R., Haber, D.A., Toner, M., 2013. Inertial Focusing for Tumor Antigen–Dependent and –Independent Sorting of Rare Circulating Tumor Cells. Sci. Transl. Med. 5, 179ra47–179ra47. doi:10.1126/scitranslmed.3005616

Petersson, F., Åberg, L., Swärd-Nilsson, A.-M., Laurell, T., 2007. Free Flow Acoustophoresis: Microfluidic-Based Mode of Particle and Cell Separation. Anal. Chem. 79, 5117–5123. doi:10.1021/ac070444e

Pethig, R., 2010. Review Article—Dielectrophoresis: Status of the theory, technology, and applications. Biomicrofluidics 4, 022811. doi:10.1063/1.3456626

Pethig, R., Menachery, A., Pells, S., De Sousa, P., 2010. Dielectrophoresis: A Review of Applications for Stem Cell Research. BioMed Res. Int. 2010, e182581. doi:10.1155/2010/182581

Pilling, D., Fan, T., Huang, D., Kaul, B., Gomer, R.H., 2009. Identification of Markers that Distinguish Monocyte-Derived Fibrocytes from Monocytes, Macrophages, and Fibroblasts. PLoS ONE 4, e7475. doi:10.1371/journal.pone.0007475

Plouffe, B.D., Mahalanabis, M., Lewis, L.H., Klapperich, C.M., Murthy, S.K., 2012. Clinically Relevant Microfluidic Magnetophoretic Isolation of Rare-Cell Populations for Diagnostic and Therapeutic Monitoring Applications. Anal. Chem. 84, 1336–1344. doi:10.1021/ac2022844

Plouffe, B.D., Murthy, S.K., Lewis, L.H., 2015. Fundamentals and application of magnetic particles in cell isolation and enrichment: a review. Rep. Prog. Phys. 78, 016601. doi:10.1088/0034-4885/78/1/016601

Poon, Z., Lee, W.C., Guan, G., Nyan, L.M., Lim, C.T., Han, J., Vliet, K.J.V., 2014. Bone Marrow Regeneration Promoted by Biophysically Sorted Osteoprogenitors From Mesenchymal Stromal Cells. Stem Cells Transl. Med. sctm.2014–0154. doi:10.5966/sctm.2014-0154

Poppema, S., Lai, R., Visser, L., Yan, X.J., 1996. CD45 (leucocyte common antigen) expression in T and B lymphocyte subsets. Leuk. Lymphoma 20, 217–222. doi:10.3109/10428199609051610

Quintanilla, R.H., Jr, Asprer, J.S.T., Vaz, C., Tanavde, V., Lakshmipathy, U., 2014. CD44 Is a Negative Cell Surface Marker for Pluripotent Stem Cell Identification during Human Fibroblast Reprogramming. PLoS ONE 9, e85419. doi:10.1371/journal.pone.0085419

Rachner, T.D., Khosla, S., Hofbauer, L.C., 2011. Osteoporosis: now and the future. The Lancet 377, 1276–1287. doi:10.1016/S0140-6736(10)62349-5

Reátegui, E., Aceto, N., Lim, E.J., Sullivan, J.P., Jensen, A.E., Zeinali, M., Martel, J.M., Aranyosi, A.J., Li, W., Castleberry, S., Bardia, A., Sequist, L.V., Haber, D.A., Maheswaran, S., Hammond, P.T., Toner, M., Stott, S.L., 2015. Tunable Nanostructured Coating for the Capture and Selective Release of Viable Circulating Tumor Cells. Adv. Mater. 27, 1593–1599. doi:10.1002/adma.201404677

Robinson, T.L., Sircar, K., Hewlett, B.R., Chorneyko, K., Riddell, R.H., Huizinga, J.D., 2000. Gastrointestinal Stromal Tumors May Originate from a Subset of CD34-Positive Interstitial Cells of Cajal. Am. J. Pathol. 156, 1157–1163. doi:10.1016/S0002-9440(10)64984-X

Ross, M.H., Pawlina, W., 2006. Histology. Lippincott Williams & Wilkins.

Saeki, K., Saeki, K., Nakahara, M., Matsuyama, S., Nakamura, N., Yogiashi, Y., Yoneda, A., Koyanagi, M., Kondo, Y., Yuo, A., 2009. A Feeder-Free and Efficient Production of Functional Neutrophils from Human Embryonic Stem Cells. STEM CELLS 27, 59–67. doi:10.1634/stemcells.2007-0980

Segré, G., Silberberg, A., 1961. Radial Particle Displacements in Poiseuille Flow of Suspensions. Nature 189, 209–210. doi:10.1038/189209a0

Shen, S., Ma, C., Zhao, L., Wang, Y., Wang, J.-C., Xu, J., Li, T., Pang, L., Wang, J., 2014. High-throughput rare cell separation from blood samples using steric hindrance and inertial microfluidics. Lab. Chip 14, 2525–2538. doi:10.1039/C3LC51384J

Shim, S., Stemke-Hale, K., Tsimberidou, A.M., Noshari, J., Anderson, T.E., Gascoyne, P.R.C., 2013. Antibody-independent isolation of circulating tumor cells by continuous-flow dielectrophoresis. Biomicrofluidics 7, 011807. doi:10.1063/1.4774304

Shi, S., Gronthos, S., 2003. Perivascular Niche of Postnatal Mesenchymal Stem Cells in Human Bone Marrow and Dental Pulp. J. Bone Miner. Res. 18, 696–704. doi:10.1359/jbmr.2003.18.4.696

Simmons, P.J., Torok-Storb, B., 1991. Identification of stromal cell precursors in human bone marrow by a novel monoclonal antibody, STRO-1. Blood 78, 55–62.

Simon, M.G., Li, Y., Arulmoli, J., McDonnell, L.P., Akil, A., Nourse, J.L., Lee, A.P., Flanagan, L.A., 2014. Increasing label-free stem cell sorting capacity to reach transplantation-scale throughput. Biomicrofluidics 8, 064106. doi:10.1063/1.4902371

Smith, J.P., Huang, C., Kirby, B.J., 2015. Enhancing sensitivity and specificity in rare cell capture microdevices with dielectrophoresis. Biomicrofluidics 9, 014116. doi:10.1063/1.4908049

Song, H., Rosano, J.M., Wang, Y., Garson, C.J., Prabhakarpandian, B., Pant, K., Klarmann, G.J., Perantoni, A., Alvarez, L.M., Lai, E., 2015. Continuous-flow sorting of stem cells and differentiation products based on dielectrophoresis. Lab. Chip 15, 1320–1328. doi:10.1039/C4LC01253D

Srisa-Art, M., Bonzani, I.C., Williams, A., Stevens, M.M., deMello, A.J., Edel, J.B., 2009. Identification of rare progenitor cells from human periosteal tissue using droplet microfluidics. Analyst 134, 2239–2245. doi:10.1039/B910472K

Stevens, A., Lowe, J., 2005. Human Histology, Third. ed. Elsevier Mosby.

Stott, S.L., Hsu, C.-H., Tsukrov, D.I., Yu, M., Miyamoto, D.T., Waltman, B.A., Rothenberg, S.M., Shah, A.M., Smas, M.E., Korir, G.K., Floyd, F.P., Gilman, A.J., Lord, J.B., Winokur, D., Springer, S., Irimia, D., Nagrath, S., Sequist, L.V., Lee, R.J., Isselbacher, K.J., Maheswaran, S., Haber, D.A., Toner, M., 2010a. Isolation of circulating tumor cells using a microvortex-generating herringbone-chip. Proc. Natl. Acad. Sci. U. S. A. 107, 18392–18397. doi:10.1073/pnas.1012539107

Stott, S.L., Lee, R.J., Nagrath, S., Yu, M., Miyamoto, D.T., Ulkus, L., Inserra, E.J., Ulman, M., Springer, S., Nakamura, Z., Moore, A.L., Tsukrov, D.I., Kempner, M.E., Dahl, D.M., Wu, C.-L., Iafrate, A.J., Smith, M.R., Tompkins, R.G., Sequist, L.V., Toner, M., Haber, D.A., Maheswaran, S., 2010b. Isolation and Characterization of Circulating Tumor Cells from Patients with Localized and Metastatic Prostate Cancer. Sci. Transl. Med. 2, 25ra23–25ra23. doi:10.1126/scitranslmed.3000403

Stroock, A.D., Dertinger, S.K.W., Ajdari, A., Mezić, I., Stone, H.A., Whitesides, G.M., 2002. Chaotic Mixer for Microchannels. Science 295, 647–651. doi:10.1126/science.1066238

Sun, T., Morgan, H., 2010. Single-cell microfluidic impedance cytometry: a review. Microfluid. Nanofluidics 8, 423–443. doi:10.1007/s10404-010-0580-9

Talary, M.S., Mills, K.I., Hoy, T., Burnett, A.K., Pethig, R., 1995. Dielectrophoretic separation and enrichment of CD34+cell subpopulation from bone marrow and peripheral blood stem cells. Med. Biol. Eng. Comput. 33, 235–237. doi:10.1007/BF02523050

Tare, R.S., Babister, J.C., Kanczler, J., Oreffo, R.O.C., 2008. Skeletal stem cells: Phenotype, biology and environmental niches informing tissue regeneration. Mol. Cell. Endocrinol., Special Issue: Stem cells and progenitors in organ maintenance, regeneration and replacement: the role of hormones and growth factors in health and disease 288, 11–21. doi:10.1016/j.mce.2008.02.017

Thege, F.I., Lannin, T.B., Saha, T.N., Tsai, S., Kochman, M.L., Hollingsworth, M.A., Rhim, A.D., Kirby, B.J., 2014. Microfluidic immunocapture of circulating pancreatic cells using parallel EpCAM and MUC1 capture: characterization, optimization and downstream analysis. Lab. Chip 14, 1775–1784. doi:10.1039/C4LC00041B

Tomer, A., 2004. Human marrow megakaryocyte differentiation: multiparameter correlative analysis identifies von Willebrand factor as a sensitive and distinctive marker for early (2N and 4N) megakaryocytes. Blood 104, 2722–2727. doi:10.1182/blood-2004-02-0769

Tong, X., Xiong, Y., Zborowski, M., Farag, S.S., Chalmers, J.J., 2007. A novel high throughput immunomagnetic cell sorting system for potential clinical scale depletion of T cells for allogeneic stem cell transplantation. Exp. Hematol. 35, 1613–1622. doi:10.1016/j.exphem.2007.06.015

Vykoukal, J., Vykoukal, D.M., Freyberg, S., Alt, E.U., Gascoyne, P.R.C., 2008. Enrichment of putative stem cells from adipose tissue using dielectrophoretic field-flow fractionation. Lab. Chip 8, 1386–1393. doi:10.1039/B717043B

Wang, X.B., Yang, J., Huang, Y., Vykoukal, J., Becker, F.F., Gascoyne, P.R., 2000. Cell separation by dielectrophoretic field-flow-fractionation. Anal. Chem. 72, 832–839.

Warkiani, M.E., Guan, G., Luan, K.B., Lee, W.C., Bhagat, A.A.S., Chaudhuri, P.K., Tan, D.S.-W., Lim, W.T., Lee, S.C., Chen, P.C.Y., Lim, C.T., Han, J., 2013. Slanted spiral microfluidics for the ultra-fast, label-free isolation of circulating tumor cells. Lab. Chip 14, 128–137. doi:10.1039/C3LC50617G

Warkiani, M.E., Khoo, B.L., Tan, D.S.-W., Bhagat, A.A.S., Lim, W.-T., Yap, Y.S., Lee, S.C., Soo, R.A., Han, J., Lim, C.T., 2014. An ultra-high-throughput spiral microfluidic biochip for the enrichment of circulating tumor cells. Analyst 139, 3245–3255. doi:10.1039/C4AN00355A

Warkiani, M.E., Khoo, B.L., Wu, L., Tay, A.K.P., Bhagat, A.A.S., Han, J., Lim, C.T., 2016. Ultra-fast, label-free isolation of circulating tumor cells from blood using spiral microfluidics. Nat. Protoc. 11, 134–148. doi:10.1038/nprot.2016.003

Xavier, M., Rosendahl, P., Herbig, M., Kräter, M., Spencer, D., Bornhäuser, M., Oreffo, R., Morgan, H., Guck, J., Otto, O., 2016. Mechanical phenotyping of primary human skeletal stem cells in heterogeneous populations by real-time deformability cytometry. Integr. Biol. doi:10.1039/C5IB00304K

Yang, L., Lang, J.C., Balasubramanian, P., Jatana, K.R., Schuller, D., Agrawal, A., Zborowski, M., Chalmers, J.J., 2009. Optimization of an enrichment process for circulating tumor cells from the blood of head and neck cancer patients through depletion of normal cells. Biotechnol. Bioeng. 102, 521–534. doi:10.1002/bit.22066

Yoon, H.J., Shanker, A., Wang, Y., Kozminsky, M., Jin, Q., Palanisamy, N., Burness, M.L., Azizi, E., Simeone, D.M., Wicha, M.S., Kim, J., Nagrath, S., 2016. Tunable Thermal-Sensitive Polymer–Graphene Oxide Composite for Efficient Capture and Release of Viable Circulating Tumor Cells. Adv. Mater. n/a–n/a. doi:10.1002/adma.201600658

Yu, M., Bardia, A., Wittner, B.S., Stott, S.L., Smas, M.E., Ting, D.T., Isakoff, S.J., Ciciliano, J.C., Wells, M.N., Shah, A.M., Concannon, K.F., Donaldson, M.C., Sequist, L.V., Brachtel, E., Sgroi, D., Baselga, J., Ramaswamy, S., Toner, M., Haber, D.A., Maheswaran, S., 2013. Circulating Breast Tumor Cells Exhibit Dynamic Changes in Epithelial and Mesenchymal Composition. Science 339, 580–584. doi:10.1126/science.1228522

Yu, M., Ting, D.T., Stott, S.L., Wittner, B.S., Ozsolak, F., Paul, S., Ciciliano, J.C., Smas, M.E., Winokur, D., Gilman, A.J., Ulman, M.J., Xega, K., Contino, G., Alagesan, B., Brannigan, B.W., Milos, P.M., Ryan, D.P., Sequist, L.V., Bardeesy, N., Ramaswamy, S., Toner, M., Maheswaran, S., Haber, D.A., 2012. RNA sequencing of pancreatic circulating tumour cells implicates WNT signalling in metastasis. Nature 487, 510–513. doi:10.1038/nature11217

Zannettino, A.C.W., Paton, S., Kortesidis, A., Khor, F., Itescu, S., Gronthos, S., 2007. Human mulipotential mesenchymal/stromal stem cells are derived from a discrete subpopulation of STRO-1bright/CD34−/CD45−/glycophorin-A-bone marrow cells. Haematologica 92, 1707–1708. doi:10.3324/haematol.11691

Zborowski, M., Sun, L., Moore, L.R., Stephen Williams, P., Chalmers, J.J., 1999. Continuous cell separation using novel magnetic quadrupole flow sorter. J. Magn. Magn. Mater. 194, 224–230. doi:10.1016/S0304-8853(98)00581-2

Zhang, B., Green, J.V., Murthy, S.K., Radisic, M., 2012. Label-Free Enrichment of Functional Cardiomyocytes Using Microfluidic Deterministic Lateral Flow Displacement. PLoS ONE 7, e37619. doi:10.1371/journal.pone.0037619

Table 2 – Current label-free microfluidic applications to stem and progenitor cell sorting. When not referred in the papers, $5x10^9$ and $5x10^6$ red and white blood cells per millilitre of blood, respectively, were considered as reference values for the performance calculations.

Reference	Sorting Method	Cell types / Sample	Throughput	Purity	Enrichment	Recovery Rate
(Srisa-Art et al., 2009)	Affinity-Based (micro-FACS)	Stro-1^+ progenitor cells from human periosteal tissue	1 µL/min 500-1,000 cells/min	N/A	N/A	N/A
(Green et al., 2009)	DLD	H1975 epithelial cells and 3T3 fibroblasts (50:50) mimicking large cardiomyocytes and smaller nonmyocytes from rat cardiac tissue digests	200 µL/min 10^5 cells/min	97%	1.9-fold	90%
(Zhang et al., 2012)	DLD	Diluted rat cardiac tissue digests (3.3×10^5 cells/mL)	80 µL /min 2.6×10^4 cells/min	91%	1.5-fold	30-35%
(Huang et al., 2008)	DLD Magnetophoresis	Nucleated-RBCs sorted from the peripheral blood from pregnant women (diluted 1:2)	216 µL/min $6x10^8$ cells/min	<0.01%	$>10^3$-fold	N/A
(Poon et al., 2014)	Inertial focusing	Larger and smaller human mesenchymal stem cells (hMSCs) from human bone marrow after culture plastic adherence	3 mL/min 3×10^6 cells/min	D^{hi} = 21.9 ± 5.3 µm; D^{lo} = 14.8 ± 2.4 µm; (Mean ± SEM)	N/A	N/A
(Hur et al., 2012)	Inertial focusing	Adrenal cortical progenitor cells from murine adrenal glands digests (4×10^5 cells/mL)	60 µL/min 2.4×10^4 cells/min	N/A	N/A	N/A
(Dykes et al., 2011)	Acoustophoresis	Peripheral blood progenitor cells separated from platelets in samples obtained by leukapheresis	20 µL/min 3.5×10^4 cells/min	< 50%	3-fold 88%-depletion of platelets	97.8%
(Lenshof et al., 2014)	Acoustophoresis	$CD4^+$ lymphocytes separated from Peripheral blood progenitor cell samples obtained by leukapheresis	30 µL/min 3×10^5 cells/min	87%	4-fold	65%
(Talary et al., 1995)	DEP	HSCs were enriched from the buffy coat of human peripheral blood and bone marrow samples	N/A	5%	~6-fold	N/A
(Wang et al., 2000)	DEP	Human haematopoietic stem cells (HSCs) from peripheral blood mixed 1:1 with a breast cancer cell line (MDA-435)	100 µL/min 1.2×10^5 cells/min	99%	~2-fold	N/A
(Simon et al., 2014)	DEP	Neural stem progenitor cells from mouse cerebral cortex fractionated into viable astrocyte progenitor-enriched populations	0.5 µL/min 2.5×10^3 cells/min	N/A	2.41-fold	N/A
(Muratore et al., 2012)	DEP	C2C12 progenitor myoblasts were separated from their progeny (myotubes) after 7 days of differentiation	2 µL/min $<8 \times 10^4$ cells/min	95% myoblasts 98.6% myotubes	~ 2-fold	N/A
(Song et al., 2015)	DEP	Immortalized human mesenchymal stem cells (hMSCs) mixed 1:1 with osteoblasts differentiated from hMSCs	0.3 µL/min 3×10^2 cells/min	84% (hMSCs) 68% (osteoblasts)	1.7-fold 1.3-fold	86% (hMSCs) 67% (osteoblasts)
(Vykoukal et al., 2008)	DEP	Pericytes/putative progenitor cells sorted from human enzyme-digested adipose tissue	1.5 mL/min $\sim 2x10^4$ cells/min	28%	14-fold	N/A
(Ling et al., 2012)	DEP	MG-63 mixed 1:3 with red blood cells	2.5 µL/min 1.3×10^3 cells/min	83%	~11.4-fold	N/A

Table 3 – Current label-free microfluidic applications to circulating tumour cell (CTC) sorting. When not referred in the papers, $5x10^9$ and $5x10^6$ red and white blood cells per millilitre of blood, respectively, were considered as reference values for the performance calculations.

Reference	Sorting Method	Cell types / Sample	Throughput	Purity	Enrichment	Recovery Rate
(Nagrath et al., 2007)	Affinity-based	4 human cancer cell lines (NCI-N1650, SKBr-3, PC3-9 and T-24) spiked (100 CTCs/mL) into whole blood Whole blood from lung, prostate, pancreatic, breast and colon cancer patients	17-34 µL/min 8.5-17x10^7 cells/min	9.2% 52-67% (depending on cancer type)	~10^9-fold	>65% Detection in 115 out of 166 patients (99%)
(Stott et al., 2010a)	Affinity-based	PC-3 cells spiked (1,000 CTCs/mL) into whole blood Whole blood from prostate cancer patients	20 µL/min 1x10^8 cells/min	14%	~10^9-fold	92% 13 to 13,167 CTCs detected in 14 out of 15 patients (93%)
(Gleghorn et al., 2010)	Affinity-based	LNCaP prostate cancer cell line spiked into whole blood Whole blood from prostate cancer patients	17 µL/min 8.5x10^7 cells/min	62-68%	~10^9-fold	85% Detection in 18 out of 20 patients
(Loutherback et al., 2012)	DLD	3 cancer cell lines (MDA-MB-231, PC3 and MCF10A) spiked (10^6 CTCs/mL) in PBS or (~7x10^6 CTCs/mL) in 1:10 diluted whole blood	10 mL/min 3x10^8 cells/min	16.7%	3.34-fold	86%
(Liu et al., 2013)	DLD	5 cancer cell lines (MCF7, MDA-MB-231, A549, HEPG2 and KYSE150) spiked (10^5 CTCs/mL) in PBS or (10^4 CTCs/mL) in 1:10 diluted whole blood	Various (50-2,000 µL/min) 9x10^8 cells/min (for 2,000 µL/min)	98.7% (for MCF7 in diluted blood, run at 2,000 µL/min)	40-fold over leukocytes 115-fold over erythrocytes (for MCF7 in diluted blood, run at 2,000 µL/min)	99% (for MCF7 in diluted blood, run at 2,000 µL/min)
(Ozkumur et al., 2013)	DLD Inertial focusing Magnetophoresis (positive selection and negative depletion)	5 cancer cell lines (MDA-MB-231, SKBR3, PC3-9, MCF10A and LBX1$^+$-MCF10A) spiked (200-1,000 CTCs/mL) into healthy whole blood Whole blood from prostate cancer patients (average of 50 CTCs/mL) Whole blood from breast cancer patients	133 µL/min 6x10^8 cells/min	7.8% (positive selection of samples from prostate cancer patients)	Total removal of RBCs 3.5 log-depletion (99.9%) of WBCs (positive selection, cytokeratins) 2.5 log-depletion (99.7%) of WBCs (negative depletion, CD45)	98.6 % (SKBR3, positive selection) 89.7% (PC3-9, positive selection) 77.8% (MDA-MB-231, positive selection) 10.9% (LBX1$^+$-MCF10A, positive selection) 97 % (MCF10A and LBX1$^+$-MCF10A, negative depletion)
(Karabacak et al., 2014)	DLD Inertial focusing Magnetophoresis (negative depletion)	6 cancer cell lines (WM164, MB231, SKBR3, PC3-9, PC9 and LBX1$^+$-MCF10A) spiked (1,000 CTCs/mL) into healthy whole blood	133 µL/min 6x10^8 cells/min	~ 50%	Total removal of RBCs 3.8 log-depletion (99.9%) of WBCs (negative depletion, CD45 + CD66b)	97%
(Bhagat et al., 2011)	Inertial microfluidics	MCF-7 cancer cell line spiked (500 CTCs/mL) into 1:20 diluted whole blood	400 µL/min 10^8 cells/min	0.025%	5.5 log-depletion of RBCs 4.1 log-depletion of WBCs	81%
(Shen et al., 2014)	Steric Hindrance and Inertial microfluidics	3 cancer cell lines (MCF-7, HeLa and K562) spiked (100-1000 CTCs/mL) in 1:40 diluted whole blood	6 µL/min 2.25x10^7 cells/min	~20%	<2.02x10^5-fold 5.3 log-depletion of blood cells	>90%
(Hou et al., 2013)	Inertial microfluidics	MCF-7 cancer cell line spiked (10^5 CTCs/mL) into 1:2 diluted whole blood Whole blood from metastatic lung cancer patients	100 µL/min 2.5x10^8 cells/min	~95% ~10%	9 log-depletion of RBCs 3 log-depletion of WBCs 9 log-depletion of RBCs 3.3 log-depletion of WBCs	85% 5 to 88 CTCs/mL recovered (detection in 20 out of 20 patients)
(Warkiani et al., 2013)	Inertial microfluidics	3 cancer cell lines (MCF-7, T24 and MDA-MB-231) spiked (<100 CTCs/mL) in 1:2 diluted RBC-lysed whole blood	1.7 mL/min 6x10^6 cells/min	<20%	~4 log-depletion of WBCs	>80%

		Whole blood from metastatic breast and lung cancer patients		N/A	N/A	6 to 57 and 3 to 125 CTCs/mL recovered in breast and lung cancer patients, respectively (detection in 10 out of 10 patients)
(Augustsson et al., 2012)	Acoustophoresis	3 prostate cancer cell lines (DU145, PC3 and LNCaP) spiked (2.5×10^5 CTCs/mL) into erythrocyte-lysed blood (10-fold diluted)	70 µL/min ~5×10^4 cells/min	97.9% (PFA-fixed DU145) 93.0% (viable DU145)	96.1% depletion of WBCs 94.9% depletion of WBCs	96.6% (PFA-fixed DU145) 83.7% (viable DU145)
(Ding et al., 2014)	Acoustophoresis	MCF-7 cancer cell line spiked (3×10^5 CTCs/mL) into RBC-lysed blood WBCs (2-fold diluted)	2 µL/min ~10^4 cells/min	84%	8.4-fold	71%
(Antfolk et al., 2015)	Acoustophoresis	DU145 prostate cancer cell line spiked (5×10^4 CTCs/mL) into erythrocyte-lysed blood (10-fold diluted)	100 µL/min ~5×10^4 cells/min	97.6% (PFA-fixed DU145)	97.6% depletion of WBCs 40-fold	95.8%
(Moon et al., 2011)	DEP	MCF-7 cells mixed with WBCs and RBCS in a 1:1:1000 proportion	126 µL/min 1.26×10^6 cells/min	16%	162-fold 99.2%-depletion of RBCs 94.2%-depletion of WBCs	76%
(Shim et al., 2013)	DEP	2 cancer cell lines (MDA-MB-435 and MDA-MB-231) spiked (50-600 CTCs/mL) into the buffy coat of healthy donors peripheral blood	250 µL/min 10^6 cells/min	70-80%	~10^4-fold	75%
		Buffy coats from late stage cancer patients		10% CTCs detected	N/A	N/A

Figure captions

Fig. 1 – Surface marker expression. Cell surface antigens of human bone marrow skeletal stem cells.

Fig. 2 – Affinity-based microfluidic cell sorting. a) (Left) Simulated prediction of cell trajectories in the equilateral triangular arrays. Red dots indicate the cells ending positions (Nagrath et al., 2007). (Right) Scanning Electron Micrograph of a captured CTC after contact with one of the functionalised micropost (Nagrath et al., 2007). b) Comparison of cell surface interactions between the herringbone chip and a flat-walled microdevice. c) Simulation of the size-dependent cell trajectories in the GEDI devices predicting the frequency of cell-obstacle collisions (Gleghorn et al., 2010). d) Size-dependent trajectories of cells flowing in GEDI devices (Kirby et al., 2012).

Fig. 3 – **Deterministic Lateral Displacement.** a) Illustration of a size-based separation in a DLD device with period N=3. In the device, cylindrical obstacles with diameter $D_{post,}$ are separated by G and the row shift fraction is given by Δλ. The micropost array divides the flow going between two posts into 3 parallel stream lines with the identical flow volumes. The width of the stream line closest to the post determines the critical size for separation (R_c). Smaller, red particles flow in zigzagging mode suffer no net total displacement. On the other hand, bigger, green particles, having its radius bigger than the critical size for separation ($R_{eff} > R_c$) are deflected at each critical decision point flowing in bumping mode and being laterally displaced at the end of the array. b) (Loutherback et al., 2012) and c) (Liu et al., 2013) show examples of the operation and principle of sheathless DLD devices. d) shows the 24 parallel DLD arrays used in the CTC-iChip to remove RBCs from whole blood (Karabacak et al., 2014).

Fig. 4 – **Magnetophoresis.** Illustration of separation by magnetophoresis. In a), a representation of magnetic-activated cell sorting (MACS). On the left, magnetic bead-conjugated antibody-labelled cells are retained in the presence of a strong magnetic field while unlabelled cells slowly flow through the device due to gravitational force. On the right, in the absence of a magnetic field, the labelled cells are collected by swiftly plunging the isolation column. In b) a representation of the quadrupole magnetic flow sorter is shown with labelled and unlabelled cells flowing in a central channel and separation occurring when a magnetic field actuates on the labelled cells driving them away from the centre of the device into a channel in the periphery, allowing separation. c) depicts the CTC-iChip in which magnetophoresis was applied to remove $CD45^+$ and $CD66b^+$ cells from whole blood, for circulating tumour cell detection (Karabacak et al., 2014).

Fig. 5 – **Inertial Microfluidics.** Phenomena in inertial microfluidics. In a) a representation of particles flowing inside a circular channel in Poiseuille flow with a typical parabolic velocity profile, shows the two dominant inertial lift forces (wall, $F_{LW,}$ and shear gradient, $F_{S\text{-}G}$) acting on the particles and drawing them onto inertial focusing equilibrium positions. In b) examples of inertial focusing positions are given for circular, square and rectangular channels. c) Representation of red blood cells flowing in a capillary evidencing the Fårhaeus-Lindqvist effect with RBCs focusing in the centre of the channel and a cell-free layer forming in the periphery. d) Formation of secondary flow Dean Vortices in a curved rectangular channel causing differential equilibrium positions for different particles given the balance of inertial lift and Dean Flows. e) Spiral microfluidic channel used to sort CTCs from RBC-lysed clinical samples (Warkiani et al., 2013).

Fig. 6 – **Acoustophoresis.** In a), the formation of a pressure node and two anti-nodes when a fundamental resonance frequency is applied with the width of the channel (w) being equal to half the wavelength of the ultrasound. In b), particles with acoustic contrast factors with opposite signs (*e.g.* red blood cells and lipid particles), are focused respectively on the pressure node and anti-nodes of the channel; In c) and d) examples of separation by acoustophoresis by a density-based, equilibrium method, and a size-based, kinetic method, respectively. e) shows a sheathless two-stage acoustophoresis device used to sort fixed DU145 CTCs spiked into RBC-lysed whole blood. The first stage pre-aligns the cells near the channel walls. At the second stage, the larger CTCs are focused faster towards the channel centre and collected in outlet 2 (Antfolk et al., 2015).

Fig. 7 – Dielectrophoresis. a) Schematic of the deflection of electric field lines by mammalian cells in a low conductivity suspending medium. On the left, the typical response to low-frequency electric fields with field lines bent around the cell creating a negative DEP force which pushes cells away from the high field region. On the right, the opposite scenario is represented with field lines drawn to the surface of the cell, resulting in a force which pulls cells towards high field regions. b) Theoretical model of the Clausius-Mossotti factor (f_{CM}) as a function of frequency for a viable cell in a suspending medium of conductivity 40 mS/m. The response of three different cells is represented which differ in size (20 or 10 µm), membrane capacitance (20 or 10 mF/m^2) or both. The following parameters were used: membrane thickness, 5 nm, nuclear envelope thickness, 40 nm, nuclear radius, 5 µm, medium relative permittivity, 78.5, membrane conductivity, 10^{-5} S/m, cytoplasm conductivity, 0.6 S/m, Nuclear envelope conductivity, $5x10^{-3}$, nucleoplasm conductivity, 2 S/m, cytoplasm relative permittivity, 60, nuclear envelope relative permittivity, 20 and nucleoplasm relative permittivity, 120. c) Schematic of a possible dielectrophoresis sorting device including a region for focusing cells, a sorting region taking advantage of different cell's dielectric properties and a trapping region using positive DEP.

Fig. 8 – Microfluidic, label-free sorting of skeletal stem cells. Possible human bone marrow skeletal stem cell sorting methodology using a combinatorial label-free microfluidic approach. The supporting table shows the main impurities and cell types found in a crude bone marrow sample along with important discriminative features such as size, cell surface markers and the ability to adhere (Alt et al., 2011; Chasis and Mohandas, 1992; Chauhan et al., 2003; Christenson and Stouffer, 1996; Freitas, 2003; Gronthos et al., 2003; Halfon et al., 2010; Junqueira and Carneiro, 2005; Kierszenbaum and Tres, 2015; Kundrotas, 2012; Lee et al., 2014; Lo Surdo and Bauer, 2012; Lv et al., 2014; May et al., 2011; Ovalle and Nahirney, 2013; Owen et al., 2013; Pilling et al., 2009; Poppema et al., 1996; Quintanilla et al., 2014; Robinson et al., 2000; Ross and Pawlina, 2006; Saeki et al., 2009; Shi and Gronthos, 2003; Simmons and Torok-Storb, 1991; Stevens and Lowe, 2005; Tare et al., 2008; Tomer, 2004). The presence of these cells on the marrow sample and after each of the 4 isolation steps is also estimated. ✓ - present; ✓ - partially depleted; ✗ - completely depleted.

Figure 1

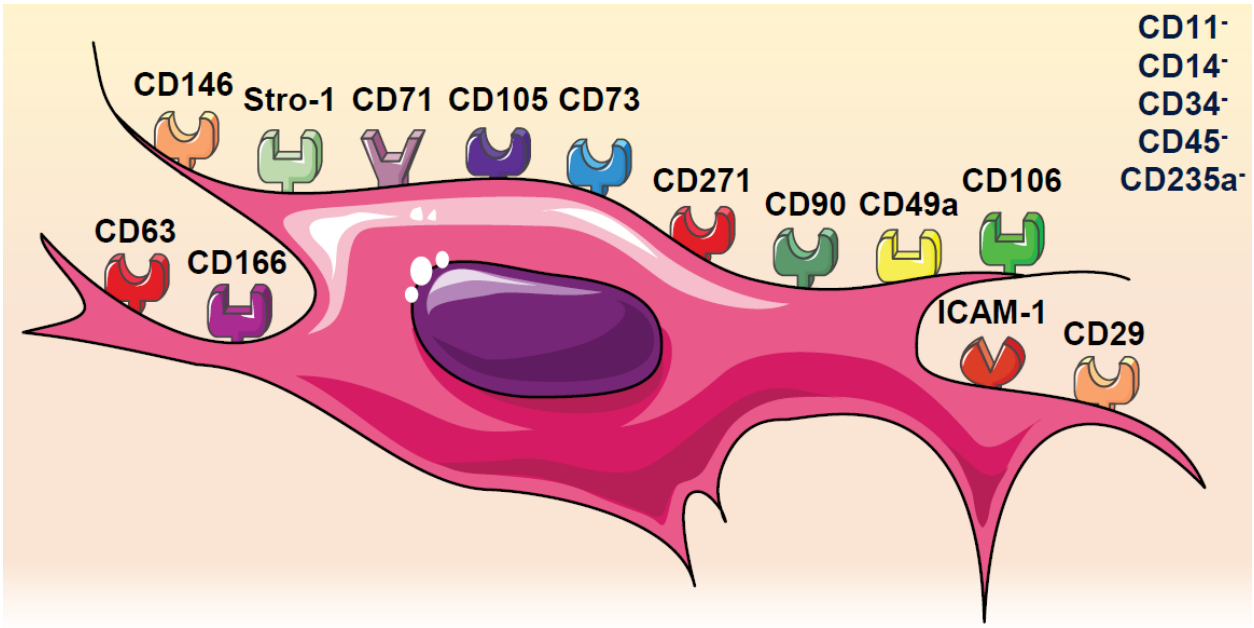

Figure 2

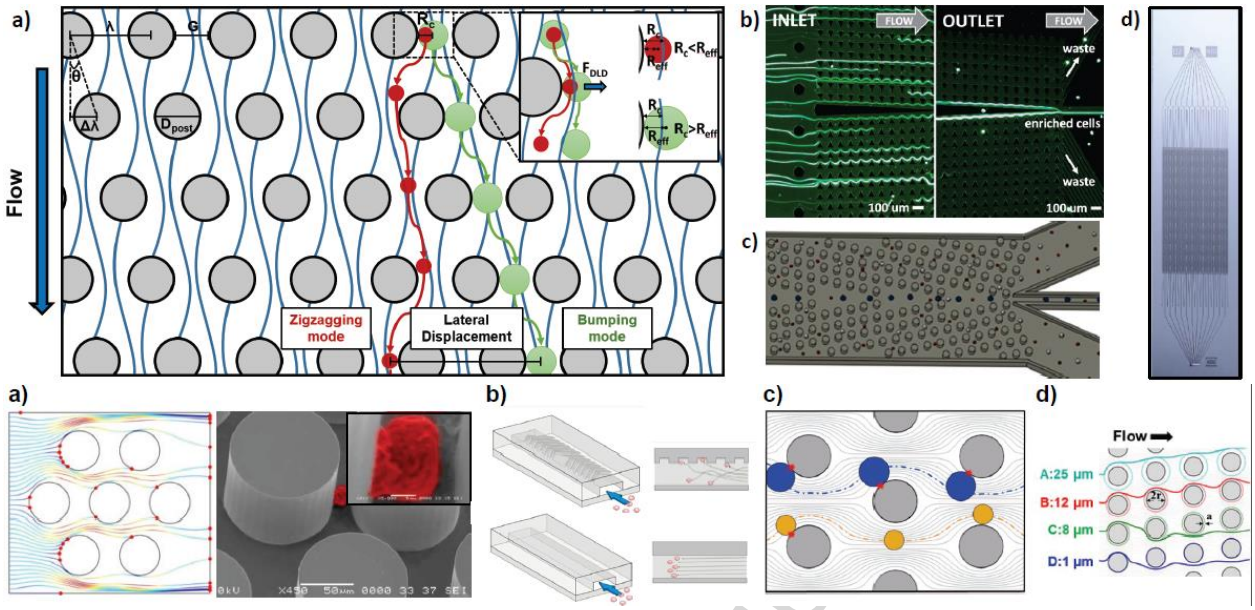

Figure 4

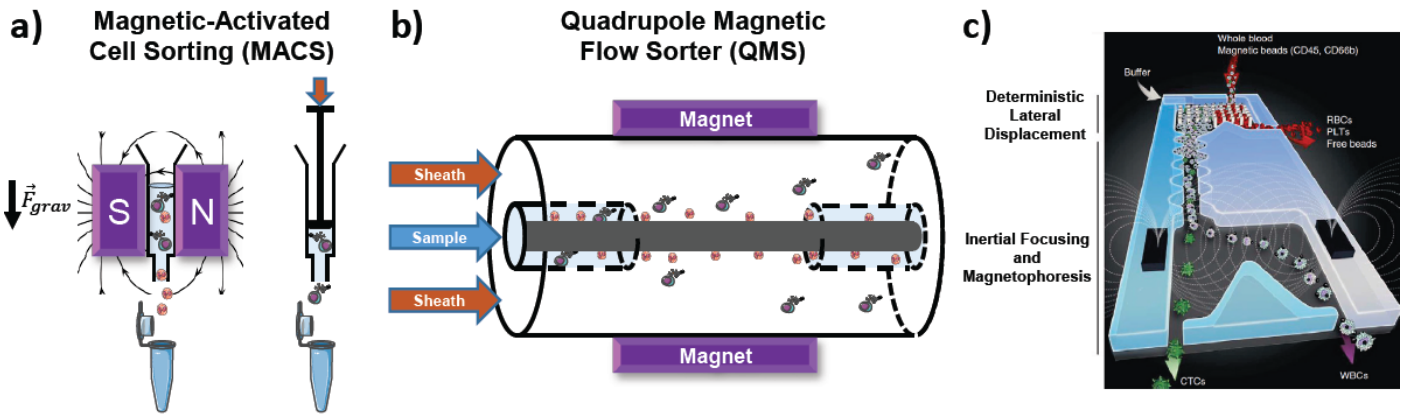

Figure 5

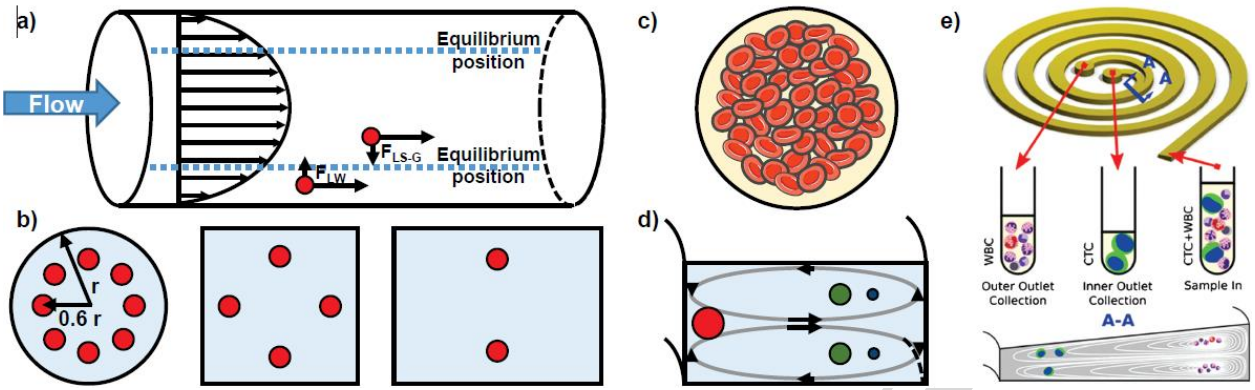

Figure 6

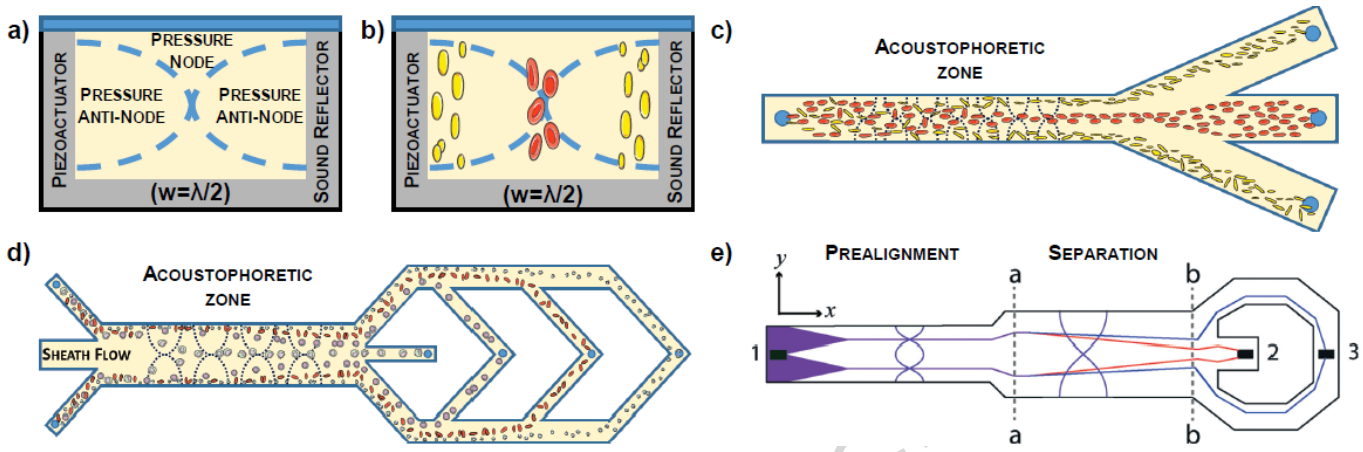

Figure 7

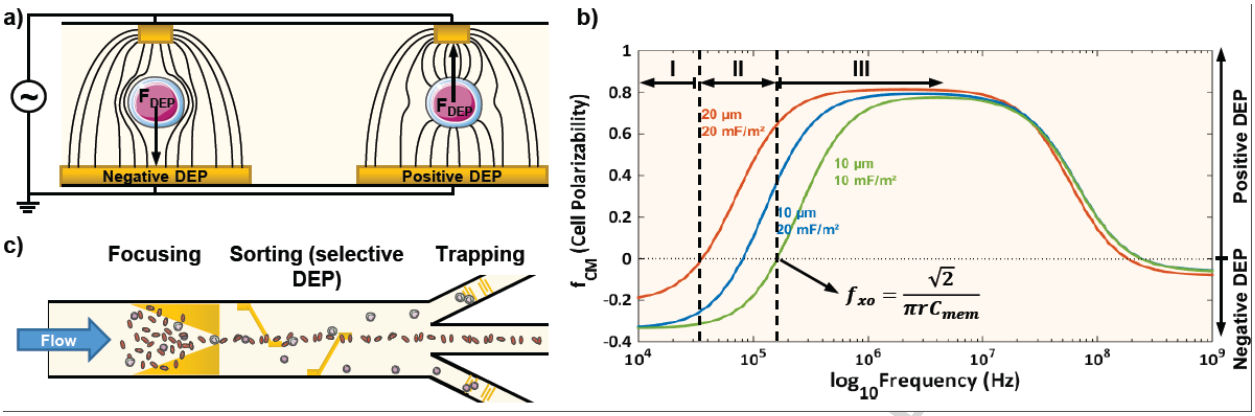

Figure 8

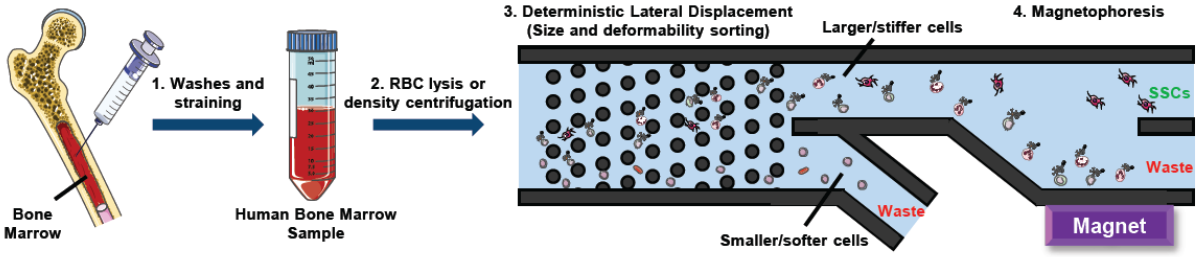

Procedure						Step 1: Washes and straining	Step 2: Erythrocyte depletion	Step 3: DLD (D_c~10μm)	Step 4: Magnetophoresis (negative selection)
Cell population/ tissue component	Name	Size (μm)	Typical cell markers	Adherent	Present in human bone marrow	After Step 1	After Step 2	After Step 3	After Step 4
	Bone debris	>40	N/A	No	✓	✗	✗	✗	✗
	Fat (yellow marrow)	N/A	N/A	No	✓	✗	✗	✗	✗
	Erythrocytes/reticulocytes	7.8 (diam.) 2.6 (thick)	GPA (CD235a)	No	✓	✓	✗/✓	✗	✗
	Platelets	2-4	CD41/CD42a/CD61	Yes	✓	✓	✓/✓	✗	✗
	Megakaryocytes	30-160	CD32/CD41/CD36/CD45		✓	✓	✓	✓	✗
	Granulocytes	12-15	CD45/CD66b	No	✓	✓	✓/✓	✓	✗
	Lymphocytes	Small (97%): 6-9 Large (3%): 9-15	CD45/CD3(T)/CD19(B)	No	✓	✓	✓	✗	✗
	NK cells	15	CD16/CD45/CD56	No	✓	✓	✓	✓	✗
	Monocytes	12-20	CD14/CD45	Yes	✓	✓	✓	✓	✗
	Erythroid nucleated cells	10-25	CD34/CD36/CD71/CD164 GPA/Stro-1	No	✓	✓	✓/✓	✓	✗
	Haematopoietic stem cells	10-30	CD45/CD34	No	✓	✓	✓	✓	✗
	Skeletal stem cells	10-25	CD34-/CD45-Stro-1/CD146	Yes	✓	✓	✓	✓	✓
	Fibroblasts	10-15	CD9/CD10/CD23/CD16 CD29/CD34/CD44/FSP-1	Yes	✓	✓	✓	✓	✗
	Vascular endothelial cells	8-12	CD31/CD34/CD106/CD146	Yes	✓	✓	✓	✓	✗

Figure 3